Western Graduate&PostdoctoralStudies

Western University
Scholarship@Western

Electronic Thesis and Dissertation Repository

4-23-2014 12:00 AM

Protein Conformational Studies by Hydrogen/Deuterium Exchange Mass Spectrometry

Antony D. Rodriguez, *The University of Western Ontario*

Supervisor: Lars Konermann, *The University of Western Ontario*

A thesis submitted in partial fulfillment of the requirements for the Master of Science degree in Chemistry

© Antony D. Rodriguez 2014

Follow this and additional works at: https://ir.lib.uwo.ca/etd

 Part of the Analytical Chemistry Commons

Recommended Citation

Rodriguez, Antony D., "Protein Conformational Studies by Hydrogen/Deuterium Exchange Mass Spectrometry" (2014). *Electronic Thesis and Dissertation Repository*. 1986.
https://ir.lib.uwo.ca/etd/1986

This Dissertation/Thesis is brought to you for free and open access by Scholarship@Western. It has been accepted for inclusion in Electronic Thesis and Dissertation Repository by an authorized administrator of Scholarship@Western. For more information, please contact wlswadmin@uwo.ca.

PROTEIN CONFORMATIONAL STUDIES BY HYDROGEN/DEUTERIUM EXCHANGE MASS SPECTROMETRY

(Thesis format: Integrated-Article)

by

Antony D. Rodriguez

Graduate Program in Chemistry

A thesis submitted in partial fulfillment
of the requirements for the degree of
Master of Science

The School of Graduate and Postdoctoral Studies
The University of Western Ontario
London, Ontario, Canada

© Antony D. Rodriguez 2014

Abstract

Proteins are biological macromolecules responsible for the majority of all physiological processes. In order to properly function proteins are required to adopt highly ordered structures. These structural aspects may be found within a single protein or arise from multi-protein complexes. Here hydrogen/deuterium exchange mass spectrometry (HDX-MS) is employed as a tool to determine the extent of protein higher order structure. Exposure to D_2O-based solvent causes the heavier isotope to exchange with amide hydrogens in the polypeptide backbone. This exchange is mainly dependent on protein conformation because the presence of stable hydrogen-bonded secondary structure will impede the incorporation of deuterium when compared to regions that are unstructured. In this work HDX-MS is used to study denaturant-induced unfolding of oxidized and reduced cytochrome *c* as well as ATP binding to the ε subunit of F_OF_1-ATP synthase. This work also lays the foundation to use this technique to study larger, more complex systems.

Keywords: hydrogen/deuterium exchange, mass spectrometry, denaturation, cytochrome *c*, ATP, ATP synthase, epsilon, ligand binding, *Escherichia coli*, *Bacillus* PS3

Statement of Co-Authorship

The work in Chapter 2 was submitted in the following articles, respectively:

> Rodriguez AD, Dunn SD, & Konermann L (2014) ATP-Induced Dimerization of the F_OF_1 ε Subunit from Bacillus PS3: A Hydrogen Exchange/Mass Spectrometry Study. Biochem. (Submitted)

The original draft of this manuscript was prepared by the author. Subsequent revisions manuscripts were done by the author and Dr. Lars Konermann. All experimental work was performed by the author, with the exception of Figure 2.7. Ms. Lee-Ann Briere of the Biomolecular Interactions and Conformations Facility (Univeristy of Western Ontario) provided the equilibrium sedimentation analytical ultracentrifugation data presented in Figure 2.7. The work in chapter 2 was done in collaboration with Dr. Stanley Dunn of the University of Western Ontario Biochemistry department.

“Our virtues and our failings are inseparable, like force and matter. When they separate, man is no more” – Nikola Tesla

Acknowledgments

Graduate school turned out to be one of the best decisions I've ever made. The exposure to scientific research in a specialized field which intrigued me made it exciting to learn again. Whether it was from conversations with colleagues to experimental trial and error, this was the academic experience I was missing. Gone were the days of simply going to class and going through the motions of everyday student life. It is this, excitement and passion I acquired over these two years that I mean most thankful for.

When I had asked Lars Konermann to take me on as a graduate student, he agreed on one condition; that I did not treat this as a contingency plan. Prior to this conversation I had told him I was not accepted into the graduate programs I had applied to. Whenever I was at an impasse with research or questioned my work, I would remember this conversation. I could not falter because I owed Dr. Konermann two years of work for what he did. I would not, and at the time of this writing have not forgotten the chance he took on me, and for that I will always be grateful.

To my colleagues past and present I thank you for the knowledge gained from our discussions. Whether it be problems with my research, or a question brought up in group meeting you were always available. A special mention to Dupe who trained me, a person who may set the record for the most proteins studied by HDX-MS in a calendar year (if there is such an achievement). Thank you as well to Dr. Stan Dunn, Yumin, and Lee-ann for the collaboration on ε and the helpful discussions. Most of all I would like to thank Siavash. In the two years of sitting beside him, I have learned more than any course, textbook or journal article would ever teach me. He pushed me at times to get things done sooner rather than later, and his knowledge of protein mass spectrometry has started to rival that of Dr. Konermann (sorry Lars). He is a professor in the making, and a good one at that. Finally I would like to thank the people outside of the lab for supporting me. My parents have always been there in the background, whether it be the odd grocery store trip or a simple phone call to see how I'm doing. To all my friends, and especially Erica, thank you for keeping me company these past two years.

Table of Contents

List of Figures

List of Abbreviations and Symbols

ADP – Adenosine 3’5’-bisphosphate

ATP – Adenosine triphosphate

AUC – Analytical ultracentrifugation

CID – Collision induced dissociation

CTD – C-terminal domain

Cyt *c* – Cytochrome *c*

D – Denaturant

ECD – Electron capture dissociation

ESI – Electrospray ionization

ETD – Electron transfer dissociation

ε –Epsilon Subunit of F_1

E_ε – ε from *Escherichia coli*

F_OF_1 – F_OF_1-ATP synthase

FerroCyt *c* – Cytochrome *c* with the Fe center in the +2 oxidation state

FerriCyt *c* – Cytochrome *c* with the Fe center in the +3 oxidation state

$\Delta G°$ – Standard Gibb’s Free Energy

GdmHCl - Guanidinium hydrochloride

^2H – Deuterium

HDX – Hydrogen/deuterium exchange

k_f – Folding rate constant

k_u – Unfolding rate constant

k_{ch} – Chemical exchange constant

k_H – Acid catalysis rate constant

k_{OH} – Base catalysis rate constant

k_{op} – Opening rate constant

k_{cl} – Closing rate constant

K – Equilibrium constant

K_{HDX} – Overall HDX constant

MS – Mass Spectrometry

m/z – Mass-to-charge ratio

MS/MS – Tandem mass spectrometry

$Na_2S_2O_4$ – Sodium dithionite

NMR – Nuclear magnetic resonance spectroscopy

NTD – N-terminal domain

Pi – Inorganic phosphate

R – Universal gas constant

T – Temperature

T_ε – ε from *Bacillus* PS3

z – Charge on the analyte

Chapter 1 – Introduction

1 Preface

Proteins are indispensable biological molecules responsible for the vast majority of physiological functions and processes. They vary in shape and size, from the smallest signalling peptide to large complexes on the order of a MDa in mass. It is the structure of proteins, through folding of higher ordered regions or assembly of larger complexes, that enable them to function. This all stems from their ability to adopt specific structures, where even the smallest deviation in bond angle would cause the protein to stagnate. Even more mysterious is that the sequence of proteins determines the 3D structure and function. This intricate and (at the present time) unresolved protein feature is the difference between a chain of random amino acids with no function and a functional biological machine (1).

One of the most commons reasons for studying protein structure is to gain insight into biological function. In order to study protein structure one must first establish the state at which the protein is to be examined, whether it be the unfolded state, native state, or some intermediate. A time frame must then be chosen because different information can be garnered at equilibrium or in kinetic experiments. Finally, the appropriate technique must be chosen to examine the structural aspects of interest.

1.1 Studying Protein Structure

1.1.1 Protein Folding

In order for a protein to function correctly it must be properly folded. This means the protein must transition from an unfolded peptide chain *U,* to a highly ordered, native structure *N*. Protein folding often a spontaneous process under native conditions where the Gibb's free energy, ΔG, is given by:

$$\Delta G = \Delta H - T\Delta S \quad (1.1)$$

There are various factors which contribute to the enthalpic (*ΔH*) and entropic (*ΔS*) terms (2). With respect to *ΔH* the formation of secondary structure upon folding introduces hydrogen bonds in *N*, however, hydrogen bonds with water must be broken in *U* before *N* can form. Entropically, the hydrophobic effect causes nonpolar regions of the protein to sequester into a core as the protein folds, thereby minimizing the formation of highly ordered "iceberg water" (3, 4). The culmination of these and other factors results in an overall spontaneous process, although the magnitude of *ΔG* is small, less than 100 kJ/mol. This small value makes it possible to convert from *N* back to *U* by manipulating temperature or solvent composition, thereby facilitating a wide range of folding experiments.

1.1.2 Equilibrium Studies

Equilibrium studies center around the notion that proteins in solution populate certain *macrostates* of varying energy, pertaining to specific conformations in a given population. The macrostates are ordered according to their free energy, and they contain a subset of structures with similar energy, deemed *microstates*. In the native state *N* the number of microstates is very low. In comparison, *U* comprises a much larger number of microstates because an unfolded protein can adopt many different structures. Other states such as intermediates can be considered additional macrostates, however, for simplicity we will only consider *N* and *U*, such that

$$U \underset{k_u}{\overset{k_f}{\rightleftarrows}} N \qquad K = \frac{[N]}{[U]} = \frac{k_f}{k_u}$$

Equilibrium experiments are often performed in the unfolding direction where a native protein is unfolded by the use of a denaturant, usually urea or guanidinium hydrochloride (5-8). The probability *P* that a protein occupies *U* follows a Boltzmann distribution

$$P_U = \frac{W_U \exp(\frac{-\Delta\varepsilon}{k_B T})}{1 + W_U \exp(\frac{-\Delta\varepsilon}{k_B T})} \tag{1.2}$$

where W_U is the number of U conformations, $\Delta\varepsilon$ is the energy difference between N and U, k_B is the Boltzmann constant, (1.38 x 10^{-23} J/K), and the denominator is the partition function, Z. Microstates of U can be consolidated by instead expressing the energy difference as ΔG:

$$W_U \exp(\frac{-\Delta\varepsilon}{k_B T}) = \exp(\ln W_U) \cdot \exp(\frac{-\Delta\varepsilon}{k_B T})$$

$$W_U \exp(\frac{-\Delta\varepsilon}{k_B T}) = \exp(-(\frac{\Delta\varepsilon - k_B T \ln W_U}{k_B T}))$$

the numerator of the exponential is similar to Eq 1.1, therefore:

$$\Delta G = \Delta H - T\Delta S \approx \Delta\varepsilon - k_B T \ln W_U$$

Eq. 1.2 can therefore be written as:

$$P_U = \frac{\exp(\frac{-\Delta G}{k_B T})}{1 + \exp(\frac{-\Delta G}{k_B T})} \tag{1.3}$$

This is the basis for many unfolding experiments because the protein can now be represented as a two-state model (5, 9). When examining macroscopic scenarios the protein stability in the presence of denaturant can be calculated according to:

$$\Delta G = \Delta G(0) - m[D] \tag{1.4}$$

where ΔG is the free energy in the unfolding direction, $\Delta G(0)$ is the free energy in the absence of denaturant, m is the measure of accessible surface area (ASA), and $[D]$ is the denaturant concentration. Because ΔG values are expressed in kJ/mol the gas constant R,

8.314 $JK^{-1}mol^{-1}$ is used instead of k_B. To determine the fraction of protein unfolded (f_U) as *[D]* increases, Eq. 1.4 is substituted into Eq. 1.3 to obtain:

$$f_U = \frac{\exp(\frac{\Delta G(0) - m[D]}{RT})}{1 + \exp(\frac{\Delta G(0) - m[D]}{RT})} \tag{1.5}$$

These unfolding curves are used to represent protein stability (Figure 1.1). A protein that is more stable requires a higher *[D]* concentration to unfold and therefore a larger ΔG in the absence of *[D]*. Protein stability can also be extended to thermal denaturation where melting curves are used (10).

1.1.3 Kinetic Studies

Proteins can be examined under kinetic conditions using trigger events such as *[D]* dilution to induce refolding. For simplicity we consider a two-state system similar to equilibrium studies where

$$U \underset{k_u}{\overset{k_f}{\rightleftarrows}} N \qquad \frac{d[U]}{dt} = -k_f[U] + k_u[N] \qquad \frac{d[N]}{dt} = -k_u[N] + k_f[U]$$

The concentration of both *U* and *N* can be calculated at any time using a 2 x 2 matrix where:

$$\begin{pmatrix} [U](t) \\ [N](t) \end{pmatrix} = \frac{d\vec{x}}{dt} = \begin{pmatrix} -k_f & k_u \\ k_f & -k_u \end{pmatrix} \vec{x} \tag{1.6}$$

$$\vec{x} = \vec{a}\exp(\lambda t) = \begin{pmatrix} a_1 \exp(\lambda t) \\ a_2 \exp(\lambda t) \end{pmatrix} \tag{1.7}$$

$$\begin{pmatrix} -k_f & k_u \\ k_f & -k_u \end{pmatrix} \begin{pmatrix} a_1 \\ a_2 \end{pmatrix} = \lambda \begin{pmatrix} a_1 \\ a_2 \end{pmatrix} \tag{1.8}$$

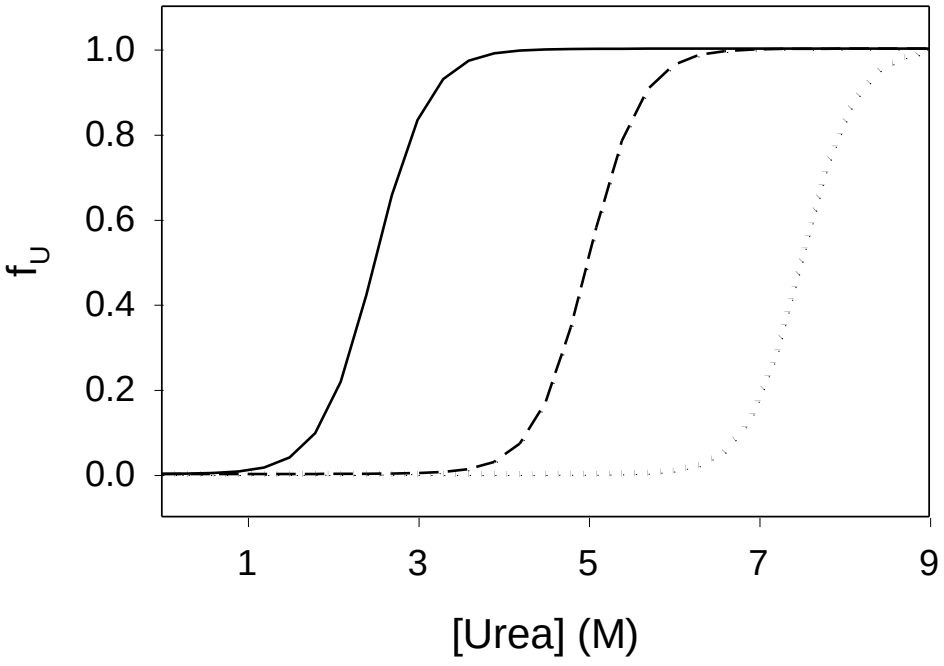

Figure 1.1 Unfolding under Equilibrium.

The increasing stability corresponds to ΔG values of -20 kJ/mol (solid line), -40 kJ/mol (dashed line) and -60 kJ/mol (dotted line).

Eq. 1.8 has the form $\hat{A}\vec{a} = \lambda\vec{a}$ where λ is the *eigenvalue* and $\vec{a}$ is an *eigenvector* of $\hat{A}$. The corresponding eigenvectors, λ_1 and λ_2 can be calculated from Eq. 1.8 so that the determinant of $\hat{A}$, det $\hat{A} = 0$. This is true for the eigenvalues:

$$\lambda_1 = -(k_f + k_u) \qquad \lambda_2 = 0$$

Substituting λ_1 and λ_2, into Eq. 1.7 one obtains the following solutions:

$$\vec{x}_1(t) = \begin{pmatrix} a_1 \exp(-(k_f + k_u)t) \\ a_2 \exp(-(k_f + k_u)t) \end{pmatrix} \tag{1.9}$$

$$\vec{x}_2(t) = \begin{pmatrix} a_1 \exp(0) \\ a_2 \exp(0) \end{pmatrix} = \begin{pmatrix} a_1 \\ a_2 \end{pmatrix} \tag{1.10}$$

Both λ_1 and λ_2 have corresponding eigenvectors, a_1 and a_2. By obtaining experimental values for k_f and k_u, a_1 and a_2 can be determined. Assuming k_f = 100 s^{-1} and k_u = 3 s^{-1} we obtain:

$$\lambda_1 = -103 \qquad a_1 = s\begin{pmatrix} -1 \\ 1 \end{pmatrix}$$

$$\lambda_2 = 0 \qquad a_2 = r\begin{pmatrix} 1 \\ 100/3 \end{pmatrix}$$

Substituting into Eq. 1.9-1.10:

$$\vec{x}(t) = \vec{x}_1(t) + \vec{x}_2(t)$$

$$\vec{x}(t) = \begin{pmatrix} [U](t) \\ [N](t) \end{pmatrix} = s\begin{pmatrix} -\exp(-103t) \\ \exp(-103t) \end{pmatrix} + r\begin{pmatrix} 1 \\ 100/3 \end{pmatrix}$$

The constants *s* and *r* depend on the initial concentrations $[U]_0$ and $[N]_0$. Assuming $[U]_0$ = 1.7 μM and $[U]_0$ = 0.3 μM we get the final solution (Figure 1.2):

$$[U](t) = 1.64\exp(-103t) + 0.006 \tag{1.11}$$

$$[N](t) = -1.64\exp(-103t) + 1.95 \quad (1.12)$$

This solution has a general formula for spectroscopic experiments:

$$S(t) = S_0 \exp(-k_{obs}t) + S_\infty \quad (1.13)$$

where k_{obs} is the observable rate constant, S_0 is the initial optical signal, and S_∞ is the signal at equilibrium. The simple two-state system described here can also be expanded to systems which include multiple intermediates and off pathways species.

1.1.4 Optical Techniques for Monitoring Protein Structure

Protein structure can be examined using a variety of optical tools. The benefits of these experiments are the ability to recover sample post analysis, as well as gain information about global changes in protein structure. These techniques, however, lack the resolution to gain information about localized structural changes. Optical measurements rely on the fact that proteins contain *chromophores*, molecules which can interact with photons through unsaturated functional groups (11). Upon exposure to the correct wavelength of light a chromophore will absorb a photon, thereby generating an electronically excited state. The relaxation of this excited state can occur non-radiatively through loss of heat or by emission of a photon. The type of photon emission depends on whether the chromophore returns to the ground state with the same spin multiplicity (fluorescence) or undergoes intersystem crossing (ISC) to a state with different spin multiplicity (phosphorescence). With respect to proteins, absorbance occurs from three different sources. The peptide bond has absorption in the far UV range (200-130 nm), however, this absorbance is often masked by co-existing species such as buffer molecules. The absorbance of aromatic amino acids, phenylalanine, tyrosine and tryptophan is most useful experimentally, with the absorbance of tryptophan at 280 nm being the most common method to determine protein concentration (12). Finally, prosthetic groups such as nucleotides (13), heme (14), or retinal (15) can be used to monitor structural changes in proteins.

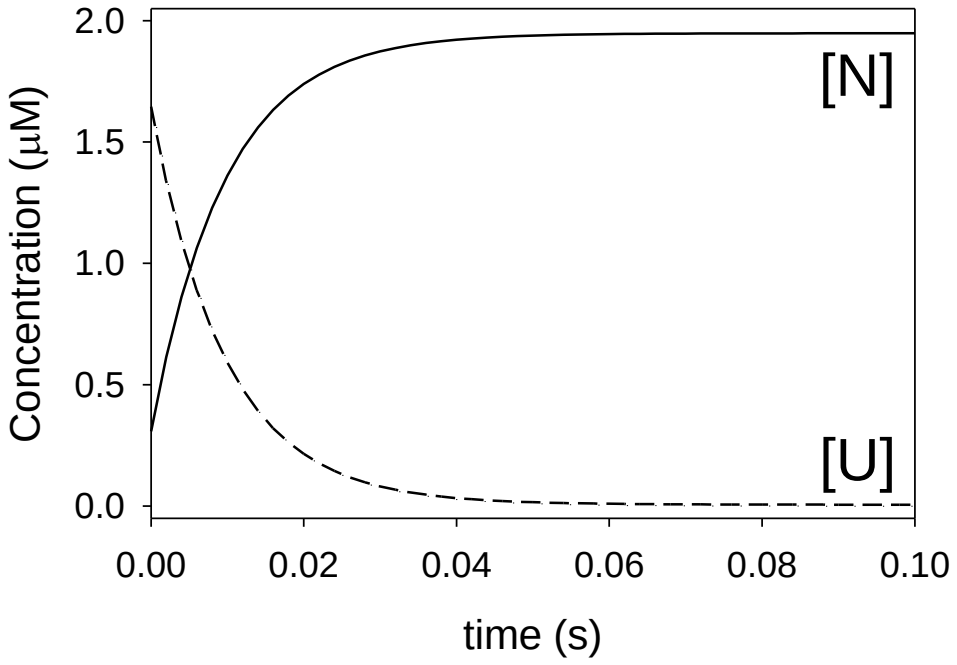

Figure 1.2 Two-State Kinetic Folding.

The concentration of [N] and [U] are plotted for a time window of 0.1 seconds. Eq. 1.11 (solid line) and 1.12 (dotted line) are plotted.

Circular dichroism (CD) spectroscopy is well suited for monitoring the extent of secondary structure in proteins (16). CD spectroscopy utilizes the difference in absorbance of both left and right circularly polarized light. Different secondary structure elements exhibit unique CD profiles. For example, a minimum at 222 nm signifies the presence of α-helical structure. Though CD spectroscopy cannot be used to explicitly determine the localized presence of secondary structure, it has been used to determine the extent to which secondary structure appears in many refolding kinetic experiments (17, 18).

1.2 Mass Spectrometry

1.2.1 Mass Spectrometry and other Analytical Tools

The use of mass spectrometry (MS) has become common practice for studying the structure of proteins (19). The strength of MS is seen primarily in its ability to complement other analytical techniques such as liquid chromatography (LC) (20-23), ultraviolet-visible spectroscopy (UV-VIS) (24), and capillary electrophoresis (CE) (25). The reduced sample consumption and cost of operation is also advantageous when compared to techniques such as nuclear magnetic resonance (NMR) spectroscopy, though MS has yet to achieve the atomic level resolution achievable by NMR (26). Furthermore, MS offers insight into protein dynamics when compared to X-Ray crystallography, though X-Ray crystallography remains to be the "gold standard" for protein structure determination (27). It is important to emphasize that mass spectrometry does not rise above any technique discussed; rather MS analysis can complement or reaffirm structural data from NMR and X-Ray crystallography. Ultimately, MS offers a different vantage point into the perplexing realm of protein conformation and dynamics.

In the following sections the different properties of mass spectrometers will be discussed, including their function and interchangeability with respect to protein analyses. At the core of the technique, MS determines the mass-to-charge ratio (*m/z*) of

charged analytes in the gas phase. In order for this to occur the mass spectrometer must be equipped with both an ion source and a mass analyzer.

1.2.2 The Ion Source

The ion source of a mass spectrometer is used to generate charged species in the gas phase. There are many different types of ion sources. A possible side effect of ionization is analyte fragmentation. Fragmentation is dependent on the properties of the ion source; softer techniques yield little to no fragmentation while harsher techniques yield abundant fragment ions (28). Soft or harsh ionization techniques can both have their advantages, however, in order to study biological macromolecules softer techniques are preferred (29). The absence of fragmentation ensures that these molecules do not lose key subdomains and that they can retain aspects of their solution phase structure.

Electrospray Ionization (ESI) is the most commonly used soft ionization technique (30). For ESI-MS analysis proteins are dissolved in a suitable solvent and injected into a narrow metal capillary (31). Upon injection the solution is electrically neutral; however the metal capillary is connected to a high voltage power supply. This voltage causes charge separation where electrons are removed from the solution (for example by solvent oxidation: $2H_2O \rightarrow 4H^+ + 4e^- + O_2$), thereby causing the accumulation of net positive charge in the solution close to the capillary tip (32). The positive charge causes distortion of the liquid at the capillary outlet into a Taylor cone (33). This Taylor cone emits a fine mist of charged droplets into the gas phase (Figure 1.3). The microdroplets are accelerated to the sampling orifice by an electric potential gradient between the capillary and the cone. In order to ensure that droplets and large contaminants do not reach the mass analyzer a counter flow of desolvation gas (often N_2) is used. Recent advancements in ESI source compartments increase ion formation by improving the trajectory to the mass analyzed and ensuring the presence of neutral species and other contaminants are minimized. Reduced sample consumption has been achieved by the introduction of nanospray capillaries (34).

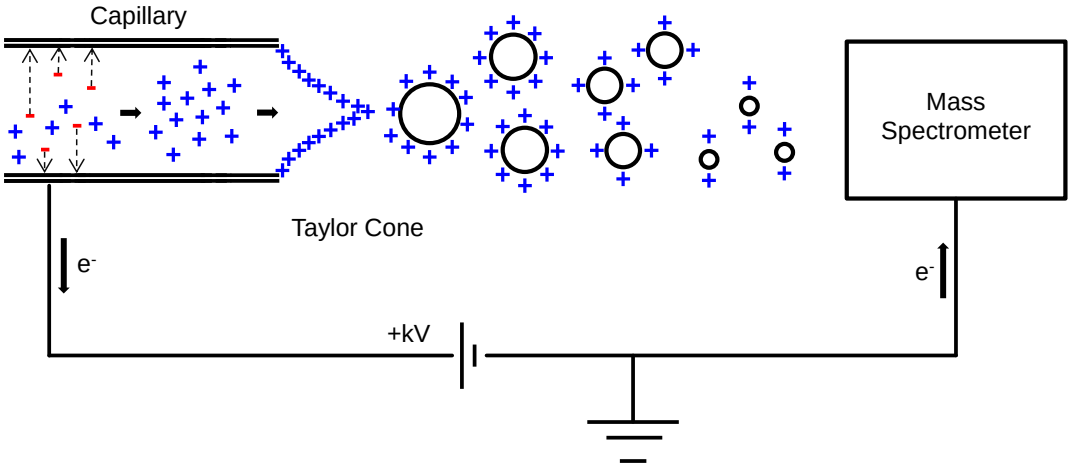

Figure 1.3 ESI-MS Scheme.

The applied voltage causes charge separation and an accumulation of positive charge. The Taylor cone formed at the end of the capillary ejects a fine mist of charged, nanoscale droplets. Constant evaporation and droplet fission creates offspring droplets on the microscale range.

The mechanism by which ESI droplets eventually produce charged analytes, $[M + zH^+]^{z+}$, has been extensively disputed (35-37). Native proteins are thought to follow the charged residue mechanism (CRM) (Figure 1.4a). The droplet charge (z) resides on the surface, and it can be approximated using the Rayleigh equation (38) according to

$$z = \frac{8\pi\left(\varepsilon_0 \gamma r_{droplet}^{\ 3}\right)^{1/2}}{e} \tag{1.14}$$

where z is the charge on the droplet, ε_0 is the vacuum permittivity, γ is the surface tension, $r_{droplet}$ is the droplet radius, and e is the elementary charge. Rapid evaporation due to high temperature causes both the droplet to shrink and charges to come close together. Due to unfavourable electrostatic repulsion of like charges the droplet undergoes jet fission and creates smaller, highly charged offspring droplets. This process of evaporation and fission proceeds to dryness wherein the final evaporation of solvent causes the remaining charge to be directly deposited onto the protein (29, 32, 39). The protein can be thought of as a protein-sized water droplet, $[M + zH]^{z+}$ where the charge is calculated according to Eq. 1.24 (40).

Though the CRM is applicable to native, compact proteins this is not the case for unfolded proteins. The chain ejection model (CEM) has been proposed to explain how unfolded proteins undergo ESI (Figure 1.4b) (37, 41). Upon formation of the charged droplet the unfolded protein chain rapidly exits the droplet while part of the surface charge transfers to the protein as it emerges. This rapid ejection is facilitated by the electrostatic repulsion of the charge distributed to the emerging chain and the remaining surface charges on the droplet. The charge transfer was observed previously using collision induced dissociation (CID) of oligomeric proteins, where the unfolded protein obtained an asymmetric amount of charge with respect to the rest of the subunits (42). Ultimately both the CRM and CEM attempt to explain the difference in charge state distribution observed in MS analysis. A third mechanism, the ion evaporation mechanism (IEM) is also used to describe ionization in the gas phase, however is pertains to small molecules (32, 43).

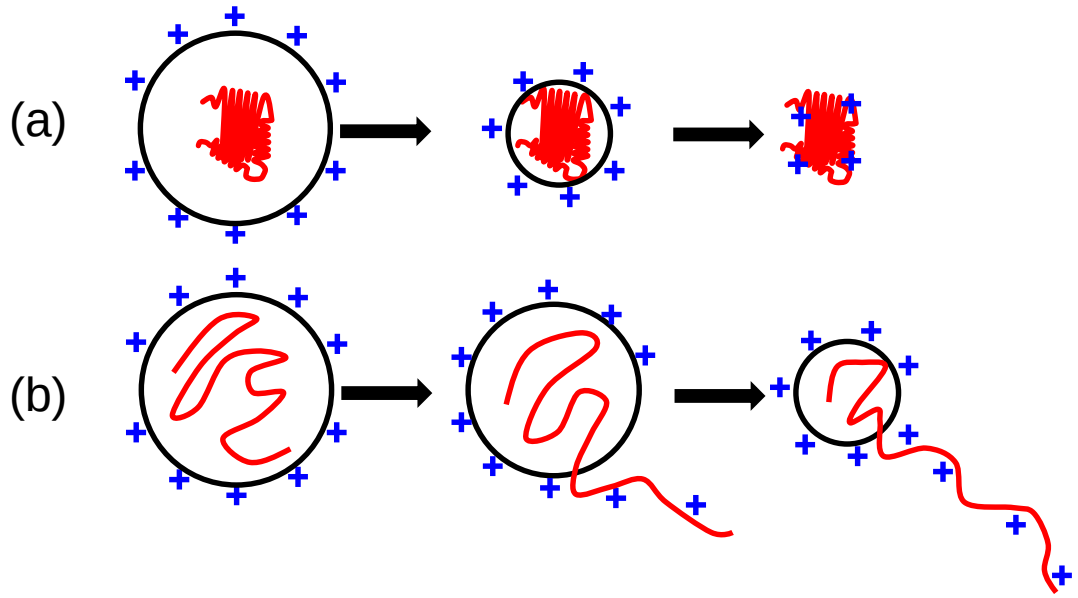

Figure 1.4 Electrospray Ionization of Proteins.

(a) Under the CRM native proteins undergo many cycles of solvent evaporation and jet fission to dryness resulting in charge transfer estimated by Eq. 1.14. (b) Unfolded proteins are thought to go through the CEM where charge is transferred from the droplet to the exiting polypeptide chain.

Matrix-assisted laser desorption/ionization (MALDI) (44) is another soft ionization source used to study proteins, however as previously mentioned ESI is more commonly used. This is because it is possible to couple LC with ESI and chromatographically separate proteins or proteolytic digestions prior to MS analysis seamlessly. MALDI predominantly yields singly charged analytes, while ESI produces multiply charged analytes.

1.2.3 The Mass Analyzer

The mass analyzer is used to determine the *m/z* of the analyte ions which is given by

$$m/z = \frac{[M + zH]}{z} \tag{1.15}$$

assuming that the entire charge is due to excess protons. Mass analyzers place a range on the allowed observable m/z. If the *m/z* of the analyte is outside this allowed range, it cannot be detected. There are many different types of mass analyzers. It is also possible to couple multiple mass analyzers in tandem to perform specific types of experiments. Mass analyzers are responsible for maximizing two key features; sensitivity and resolution. They must be sensitive enough to detect analytes even at low concentration and be able to distinguish between analytes of similar mass. Resolution, *R* is defined as

$$R = \frac{M}{\Delta M} \tag{1.16}$$

where ΔM is the full width at half maximum (FWHM) for each respective peak.

There are many types of mass analyzers found in mass spectrometers however only quadrupoles and TOF systems will be discussed in detail. It is important to note, however, that linear ion traps (45), the Orbitrap (46-48), and Fourier transform ion cyclotron resonance (FT-ICR) (49) mass analyzers are also commonly used.

1.2.3.1 Quadrupole Mass Analyzers

The most common mass analyzer found in mass spectrometers is the quadrupole. Single quadrupoles have been used to study proteins in the past; however, they are limited by small *m/z* ranges especially when used alone (50-54). A quadrupole is comprised of two pairs of charged cylindrical metal rods, one pair positively charged and one negatively charged. These metal rods are aligned so that the charged pairs face one another. At all times a radio frequency (RF) voltage is applied to the quadrupole; however the inclusion of direct current (DC) voltage can be used to change the observable *m/z* range. Ions travel from the source through the quadrupole. With only the RF voltage applied, all charged ions will pass through the quadrupole (Figure 1.5.a). However, the *m/z* range can be narrowed by superimposing DC voltage onto the RF voltage. Only ions of a certain *m/z* value will reach the detector for a given RF/DC voltage ratio by having the correct trajectory (Figure 1.5.b). When the DC voltage is applied all other charged analytes will collide with the charged rods because their trajectories are unstable.

1.2.3.2 Time-of-Flight Mass Analyzers

Time-of-flight (TOF) mass analyzers cover a much larger *m/z* range than quadrupoles. TOFs are also able to record all ions striking the detector without scanning. This is unlike a quadrupole which must scan the entire mass range set by the respective RF voltage, resulting in a lower duty cycle. TOF instruments work by measuring the time an analyte takes to reach a detector after it has entered the flight tube. When an ion is accelerated by a voltage, U, the potential energy, E_p is converted into kinetic energy, E_k such that $E_p = E_k$ and

$$E_p = zU \qquad E_k = \frac{1}{2}mv^2$$

$$zU = \frac{1}{2}mv^2 \tag{1.27}$$

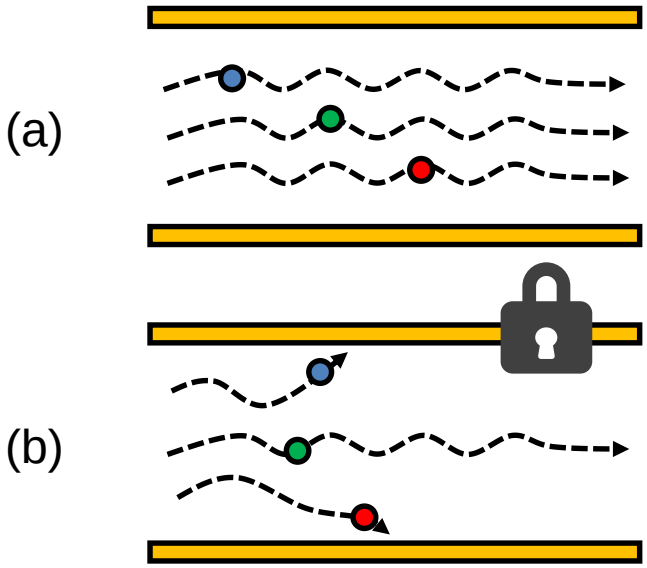

Figure 1.5 Schematic: Quadrupole Operation.

(a) With only RF voltage applied all ions (coloured circles) can pass through to the detector. (b) The application of DC voltage "locks" the quadrupole so that only ions with a specific *m/z* (green circle) can pass through, while all others hit the charged rods.

where *m*, *z* and *v* are the mass, charge and velocity of the ion. After the ions are accelerated they have the *same velocity* as they travel in a field-free region towards the detector, therefore the time it takes to reach the detector can be described as:

$$zU = \frac{1}{2} m \frac{v^2}{t^2}$$

$$t = k\sqrt{\frac{m}{z}} \tag{1.18}$$

Where *k* are the parameters independent of the analyte:

$$k = \frac{d}{\sqrt{2U}}$$

From Eq. 1.18 it is clear the time it takes to travel in the TOF instrument depends on the *m/z* of the ion. Orthogonal versions of the traditional linear TOF geometry have become standard (55). Slight deviations in velocity cause ions of similar mass to arrive at the detector with different flight times, thereby decreasing resolution. Most TOFs therefore use a reflectron, i.e. a stacked set of rings with a potential applied. Upon entering the TOF tube the ions are first pushed perpendicularly by a potential drop ("pusher pulse") towards the reflectron (Figure 1.6.a). Even if two ions have the same *m/z* ratio their velocities may deviate slightly, therefore the ion travelling at a faster velocity will penetrate the reflectron first but dwell longer before its trajectory is reflected towards the detector (Figure 1.6.a). The slower ion will penetrate the reflectron later but the reflectron will spend less time changing the ion trajectory. Overall this dwell corrects the velocity deviation and the two ions will reach the detector at the same time. The reflectron correction can be described as two balls of similar mass rolling up a ramp at different velocities, according to Figure 1.6.b.

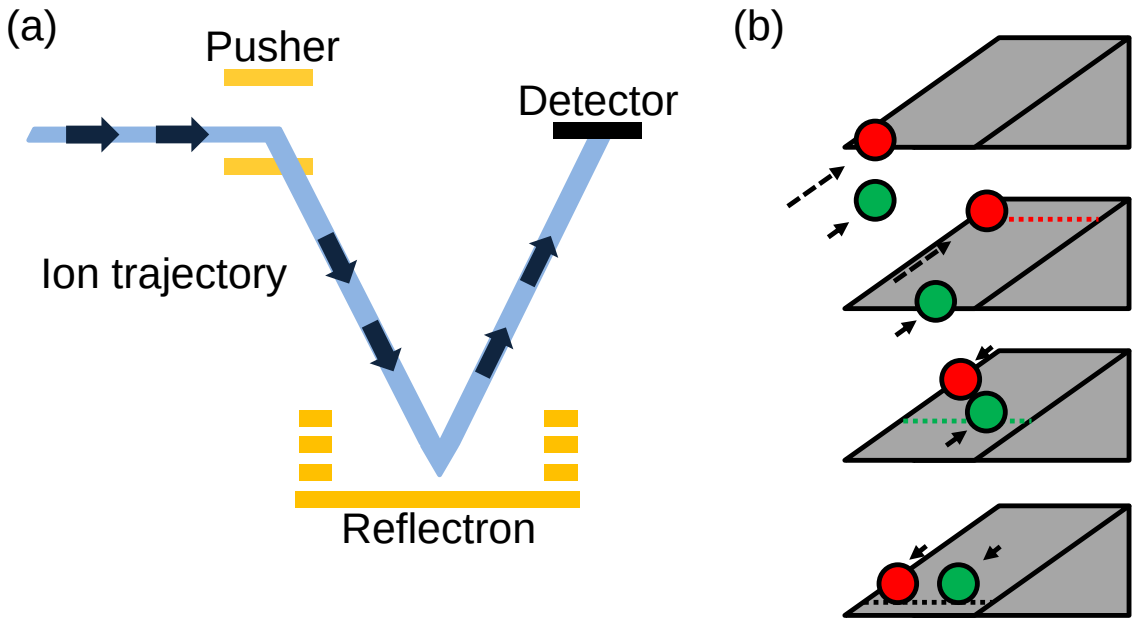

Figure 1.6 Orthogonal TOF Schematic.

(a) The pusher sends the ions towards the reflectron which changes the trajectory towards the detector, correcting any deviation in flight time. (b) The faster moving red ball hits the ramp first but travels further up (red dotted line), while the slower moving green ball hits the ramp last but does not travel up as far (green dotted line). The time delay is corrected and ultimately the two balls exit the ramp at the same time.

1.2.4 Structural Mass Spectrometry

Mass spectrometry has become especially useful when looking at protein structure. Many of these techniques employ a "bottom-up" approach whereby information on structure is gained by examining smaller pieces or fragments of the protein. CID and tandem mass spectrometry (MS/MS) are used to sequence proteins by proteolytic digestion followed by peptide identification. For MS/MS the potential across the quadrupole is increased causing the peptide to collide with background gas and fragment into smaller ions which provide sequence information (56). Sequencing is also assisted by the presence of neutral loss fragments (H_2O and NH_3) and immonium ions. All of the fragments are detected by the TOF analyzer. Fragmentation can also be induced by electron capture dissociation (ECD) or electron transfer dissociation (ETD). In ECD free electrons are transferred to the peptide (57-60), while ETD employs radical anions to trigger fragmentation (61-64).

Peptide fragmentation is a gas-phase phenomenon that has been extensively discussed in literature; however the mechanism by which these fragments are formed has not been resolved (65-69). Fragments that arise from CID are formed from bond breakage between the amide nitrogen and carbonyl carbon in a protein sequence (Figure 1.7). If the charge remains on the segment with the newly formed C-terminus it is denoted as a *b*-ion and if it remains with the newly formed N-terminus it is denoted as a *y*-ion (Figure 1.7). Fragmentation using ECD/ETD occurs with bond breakage between the amide nitrogen and alpha carbon, producing *c*-ions (charge on C-terminus) and *z*-ions (charge on N-terminus) (58, 61, 70, 71). The identification of these peptide fragments can be especially useful when a non-specific protease is used for digestion (72-75).

Protein structure can also be studied in the gas phase and compared to solution phase structure using ion mobility spectrometry (IMS) (76). In IMS experiments proteins travel through a collision cell that is filled with background gas. The drift-time of the protein as it travels is rated to the gas phase conformation by its collision cross section, Ω. Ω is the average area the protein contacts the gas in the collision cell.

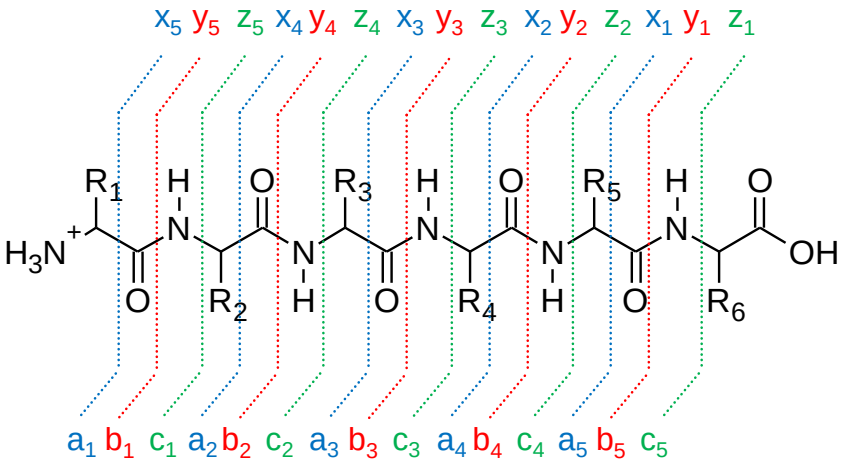

Figure 1.7 Peptide Fragmentation Scheme.

CID induces *b*/*y*-ion fragmentation between the amide nitrogen and carbonyl carbon (red) while ECD/ETD induce *c*/*z*-ion fragmentation between the amide nitrogen and alpha carbon (green). The presence of *a*/*x*-ion fragmentation is rare and occurs between the alpha carbon and carbonyl carbon (blue).

Proteins with native-like structure are compact and therefore have small Ω while unfolded proteins which can adopt various conformations have larger Ω values.

1.3 Hydrogen/Deuterium Exchange Mass Spectrometry

1.3.1 HDX Fundamentals

The exchange of a hydrogen atom with deuterium (^{2}H) in a D_2O-containing solvent occurs at both the amide backbone of the protein as well as any nitrogen, oxygen, or sulfur containing side chain groups (77). The intramolecular hydrogen bonding associated with the backbone is of primary intent for HDX-MS as it provides information on secondary structure. Side chain sites will not be discussed any further, because they undergo back-exchange during chromatographic separation.

We will first focus on HDX of a completely "open" backbone amide site that is completely accessible and not involved in hydrogen bonding. The chemical exchange process of such a site can be either acid or base catalyzed with the rate (k_{ch}) being equal to

$$k_{ch} = k_H[H^+] + k_{OH}[OH^-] \tag{1.19}$$

where k_H and k_{OH} are rate constants for acid and base catalysis (78-80). The values of k_H and k_{OH} depend on the adjacent amino acid side chains. Eq. 1.19 dictates that k_{ch} is highly dependent on the pH (or pD) of the solution (Figure 1.8) (81). Similar sensitivity to temperature is also evident in k_{ch} as it follows the Arrhenius equation

$$k_{ch} = A\exp(-\frac{E_a}{RT}) \tag{1.20}$$

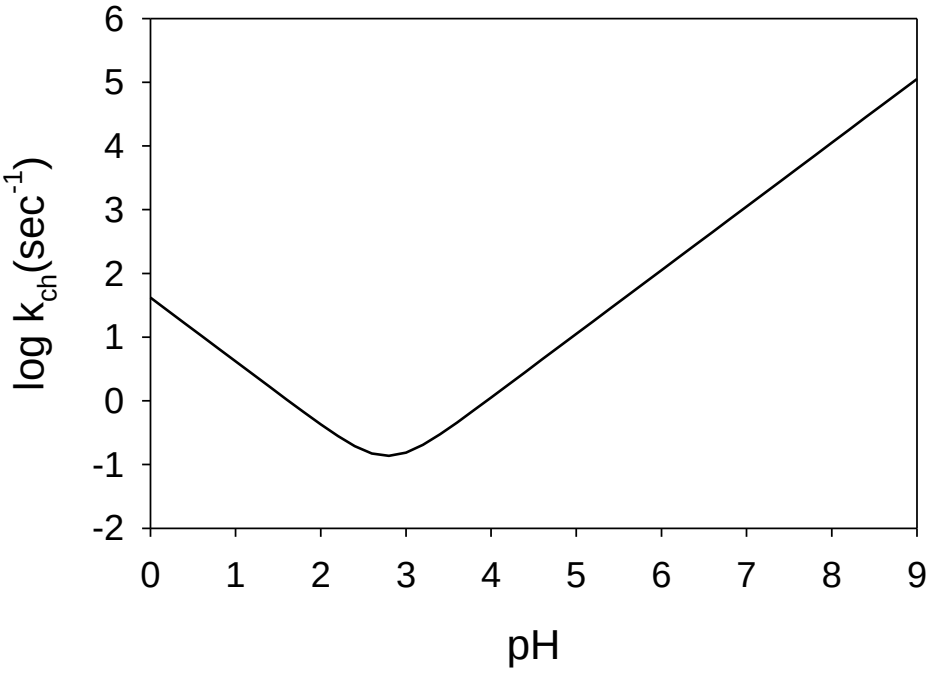

Figure 1.8 pH Sensitivity of k_{ch}.

The chemical exchange rate constant of polyalanine as a function of pH exhibits a minimum at ~ 2.7. The k_H and k_{OH} values were 41.7 and 1.12 x 10^{10} M^{-1} min^{-1} at 20°C (81).

1.3.2 The EX1 and EX2 Regime

At the protein level, exchange rate constants are generally much lower than predicted on the basis of Eq. 1.19. This is due to the partial protection of hydrogens by secondary and tertiary structure formation, where a decrease by as much as 10^8 can be observed. For deuterium exchange to take place there must be a transient moment where the hydrogen bond donor and acceptor must be transiently separated, effectively opening the hydrogen bond (82). This enables deuterium incorporation into the backbone according to

$$H_{cl} \underset{k_{cl}}{\overset{k_{op}}{\rightleftarrows}} H_{op} \xrightarrow[D_2O]{k_{ch}} D_{op} \underset{k_{op}}{\overset{k_{cl}}{\rightleftarrows}} D_{cl} \tag{1.21}$$

where H_{op} and H_{cl} are the open and closed hydrogen bond, D_{op} are the open and closed deuterium bond and k_{op} *and* k_{cl} are the opening and closing rate constants. The exchange reaction is unidirectional if the amount of deuterium remains in excess. If we consider both H_{op} and H_{cl} as a single *unexchanged* entity then:

$$\frac{d[unexchanged]}{dt} = -k_{ch}[H_{op}] \tag{1.22}$$

$$\frac{d[H_{op}]}{dt} = -(k_{cl} + k_{ch})[H_{op}] + k_{op}[H_{cl}] \tag{1.23}$$

If we assume that the rates of formation and depletion for H_{op} are equal ($\frac{d[H_{op}]}{dt} \approx 0$):

$$(k_{cl} + k_{ch})[H_{op}] = k_{op}[H_{cl}]$$
$$(k_{cl} + k_{ch})[H_{op}] = k_{op}([unexchanged] - [H_{op}])$$

$$[H_{op}] = \frac{k_{op}}{k_{cl} + k_{ch} + k_{op}}[unexchanged] \tag{1.24}$$

If we substitute this into Eq. 1.22 we obtain a pseudo first order expression:

$$\frac{d[unexchanged]}{dt} = -\frac{k_{op}k_{ch}}{k_{cl} + k_{ch} + k_{op}}[unexchanged] \tag{1.25}$$

$$[unexchanged] = \exp(-k_{HDX}t) \tag{1.26}$$

where:

$$k_{HDX} = \frac{k_{op}k_{ch}}{k_{cl} + k_{ch} + k_{op}} \tag{1.27}$$

If the amide hydrogen remains predominantly hydrogen bonded with only transient moments where the bond is broken, then $k_{cl} >> k_{ch}$ and the overall HDX rate (k_{HDX}) is given by

$$k_{HDX} = K_{op}k_{ch} \tag{1.28}$$

where $K_{op} = (k_{op}/k_{cl})$ is the equilibrium constant of the opening reaction. This is known as the EX2 regime which most proteins fall under (Figure 1.9). Under these conditions the probability of backbone sites being exchanged in a single opening event is very small. Therefore the incorporation of deuterium is the result of numerous opening/closing cycles. In the EX2 regime the amount of deuterium incorporated and therefore the degree in mass shift is time dependent. While there are proteins that exhibit the EX1 behaviour ($k_{ch} >> k_{cl}$), such cases are rare. Such conditions can be encountered in solvents that destabilize the native state (decreasing k_{cl}) or the use of basic conditions with high pD (increasing k_{ch}). Sample carryover can sometimes be mistaken as EX1 kinetics (83).

1.3.3 Hydrogen/Deuterium Exchange Mass Spectrometry

Hydrogen/deuterium exchange mass spectrometry (HDX-MS) is a relative new method for studying protein structure and dynamics (84, 85). Under native conditions, the majority of proteins in any given population occupy the lowest energy native state. However, due to the dynamic nature of proteins a small fraction of the population

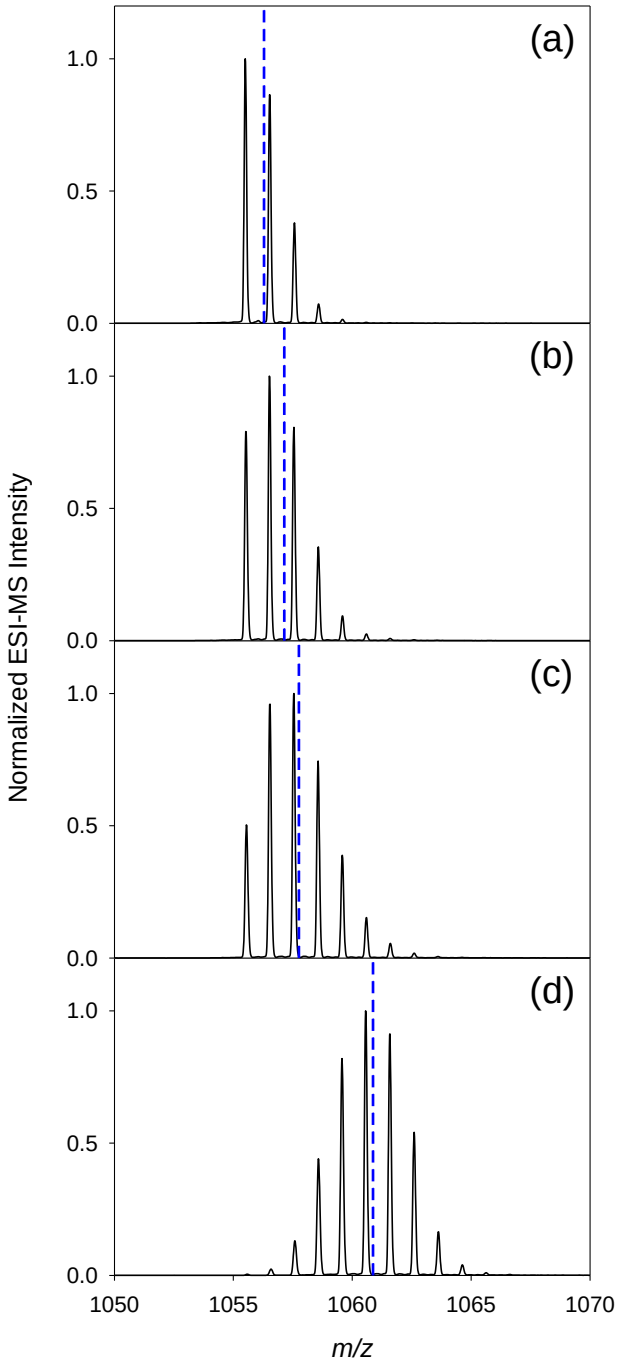

Figure 1.9 Deuterium Uptake in the EX2 Regime.

Peptide mass spectra (m/z = 1055.738 1+) in the absence of deuterium (a), after exposure to D_2O for 1 min (b) and 10 min (c). The dashed line indicates the centroid of the mass distribution. Panel (d) shows the fully deuterated peptide.

transiently samples higher energy states at all times before returning back to the native state. At these higher energy states the structure of the protein differs greatly from the native state; certain regions may unfold and hydrogen bonds may be open (Figure 1.10a). It is possible to determine extent to which proteins occupy these higher energy levels by HDX (86-92). The degree at which a protein deviates from the native state structure when sampling higher energy levels will be seen in the degree of deuterium uptake. In the presence of D_2O all the amide backbone hydrogens of a protein will eventually exchange with deuterium. The rate at which this exchange occurs can be attributed primarily to the degree of flexibility in the secondary structure of the protein as well as small contributions in solvent accessibility according to Eq. 1.21 (93). Highly ordered regions such as α-helices and β-sheets exchange at a slower rate than regions that are unstructured. This idea can be extended to protein-ligand binding studies. Ligands are known to stabilize protein structure. Therefore upon inclusion of a ligand, the protein equilibrium would follow Le Chatelier's Principle and shift towards the ligand-bound state (Figure 1.10.b). This shift consequently reduces the percentage of proteins that sample higher energy states and in the HDX analysis would be observed as a reduction in deuterium uptake.

Continuous HDX-MS experiments are performed as follows: Intact protein is first exposed to D_2O under conditions where the protein is native (pH 7, 25°C) (Figure 1.11). Aliquots are then taken at desired time points where the exchange reaction is quenched by rapidly decreasing the pH and temperature (pH 2.3, 0°C) (94). Proteins can be examined intact, or they can be proteolytically digested for spatially-resolved studies by an acid protease such as pepsin. An acid protease is required because other enzymes such as trypsin cannot function at the low pH required for quenching. Pepsin digestion has initially been done in solution, until the manufacturing of immobilized pepsin columns designed for high pressure liquid chromatography (HPLC) were introduced (72, 75, 95, 96). The separation of peptic fragments prior to MS using online HPLC has become a standard approach. There is, however, problem with this approach because deuterated amides can undergo back-exchange during the separation process (97). In order to minimize back-exchange the system is cooled to 15°C during digestion and it is further cooled to 0°C during separation (98).

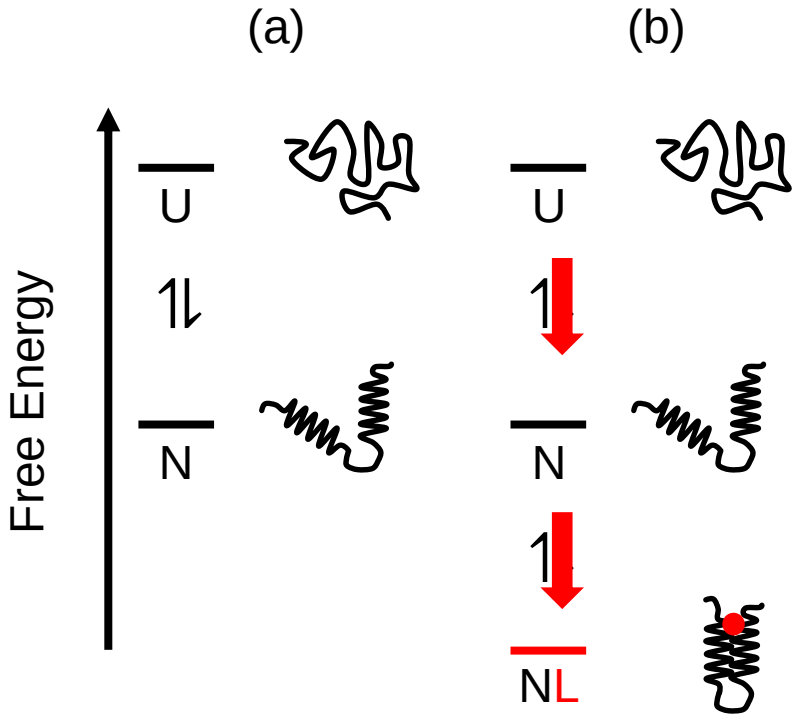

Figure 1.10 The Dynamic Equilibrium of Proteins.

(a) Under native conditions proteins are in equilibrium with the native state (N) and higher energy states, such as the unfolded state (U). (b) Incorporation of a ligand (red circle) shifts the equilibrium from these higher energy states to the new ground state NL.

The HPLC gradient is also optimized to minimize retention time without sacrificing resolution. Reverse-phase HPLC is used to separate peptide fragments with acetonitrile acting as the organic eluent. The peptides are finally analyzed online by ESI-MS where the incorporated deuterium and the resulting mass shift can be observed. Recent developments in ultra-high performance liquid chromatography (UPLC) as well as semi and fully automated LC machinery have further refined the HDX workflow. It is important to note that HDX-MS can also be used to study protein kinetics (99). *Pulsed* HDX-MS has been used in refolding experiments to gain insight into protein folding by briefly exposing the protein to deuterium as it refolds on the millisecond time scale (100-102). Consequently regions which show less deuteration are indicative of secondary structure formation along the folding pathway.

HDX-MS does present certain limitations when examining protein structure. Experimentally, spatially resolved analysis of HDX kinetics requires peptide identification using a non-specific protease. Typical proteases with known cleavage sites such as trypsin (103) are not utilized because the cleavage process cannot be done at the low pH required for HDX-MS experiments. Therefore pepsin or other non-specific proteases which can undergo proteolytic cleavages under acidic conditions are employed (96). The protein size must also be considered because of the magnitude of peptides generated by proteolysis, followed by the time consuming process of identifying each peptide correctly. Recently, the time invested in peptide identification has been dramatically decreased due to software improvements (104). The temperature sensitive exchange process can also become problematic during peptide separation, as structural information can be lost due to back-exchange with the HPLC solvent.

Limitations also arise when HDX-MS is often to study protein/ligand systems. Ligand binding usually stabilizes the protein and induces a reduction in HDX rates. The largest changes tend to occur in regions that interact directly with the ligand, although allosteric effects can play a role as well (90, 105). Low affinity often results in indistinguishable kinetics with respect to the ligand-free and ligand-bound scenarios. In this way, using HDX-MS to determine structural changes is limited by the strength of the protein/ligand interaction.

1.4 Scope of this Thesis

Here we employ HDX-MS as a tool for studying two different protein systems. HDX at backbone sites that are involved in α-helices and β-sheets is much slower than an unfolded region. Deuteration at these sites is mediated by conformational fluctuations that induce the transient opening of hydrogen bonds, coupled with exposure of N-H sites to the solvent. Thus, HDX in flexible regions proceeds much faster than in rigid segments. The flexibility of the technique, as well as the various degrees of structural information which can be elucidated will be highlighted.

Spatially resolved HDX-MS is used to characterize structural changes upon ligand binding (Chapter 2). This work examines two different systems with various affinities to a common ligand. Ligand binding influences the magnitude by which HDX kinetics are changed, therefore the observed binding affinities previously determined using NMR spectroscopy are compared to the HDX kinetics of the ligand-bound and ligand-free states. The hypothesis of higher ordered structure formation upon ligand binding is also presented, with the generated HDX-MS data acting as crucial evidence.

Intact HDX-MS is used to characterize the structural changes of a redox-active protein (Chapter 3). Redox-active proteins can undergo reversible oxidation and reduction reactions, resulting in minimal changes to the structure as a whole. Therefore, HDX-MS is used to detect these small fluctuations in structure and, ultimately push the limits of this technique. Chemical denaturation is used in conjunction with HDX-MS in an attempt to selectively locate regions of the protein which are more susceptible to unfolding by examining the HDX kinetics in the presence of increasing denaturant concentration. At low denaturant concentrations certain regions of the protein are easily unfolded, while others may resist unfolding due to strong secondary structure interactions. This translates to an increase in the HDX kinetics between the oxidized and reduced states of the redox-active protein as the denaturant concentration is increased. Provided the concentration is low enough to selectively, and not globally, unfold the protein, HDX-MS in tandem with chemical denaturation may be useful in examining protein systems with subtle structural changes.

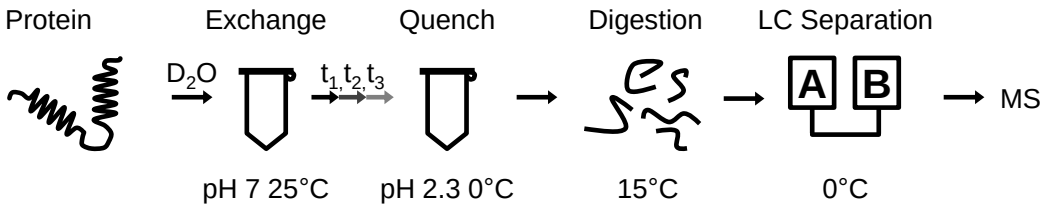

Figure 1.11 Schematic Overview of an HDX-MS Experiment.

Aliquots are first digested by immobilized pepsin and then separated using reverse-phase HPLC. Solvent A and B are HPLC solvents used for peptide separation with B being the organic solvent such as acetonitrile.

1.5 References

1. Anfinsen CB (1973) Principles that Govern the Folding of Protein Chains. *Science* 181:223-230.

2. Dill KA & MacCallum JL (2012) The Protein-Folding Problem, 50 Years On. *Science* 338:1042-1046.

3. Bakker HJ (2012) response to the fear of water. *Nature* 491(7425):533-535.

4. Southall NT, Dill KA, & Haymett ADJ (2002) A View of the Hydrophobic Effect. *J. Phys. Chem. B* 106:521-533.

5. Konermann L (2012) Protein Unfolding and Denaturants. in *eLS. John Wiley & Sons, Ltd* (Chichester).

6. Greene RF & Pace CN (1974) Urea and Guanidine Hydrochloride Denaturation of Ribonuclease, Lysozyme, α-Chymotrypsin, and β-Lactoglobulin. *J. Biol. Chem.* 249:5388-5393.

7. Knapp JA & Pace CN (1971) Guanidine Hydrochloride and Acid Denaturation of Horse, Cow, and Candida krusei Cytochromes c. *Biochemistry* 13:1289-1294.

8. Pace CN & Vanderburg KE (1979) Determining Globular Protein Stability: Guanidine Hydrochloride Denaturation of Myoglobin. *Biochemistry* 18:288-292.

9. Fersht AR (1999) *Structure and Mechanism in Protein Science* (W. H. Freeman & Co., New York).

10. Privalov PL & Khechinashvili NN (1974) A Thermodynamic Approach to the Problem of Stabilization of Globular Protein Structure: A Calorimetric Study. *J. Mol. Biol.* 86:665-684.

11. Schmid FX (2001) Biological Macromelecules: UV-Visible Spectrophotometry,. *In Encyclopedia of life Science, Nature Publishing Group: London*.

12. Pace CN, Vajdos F, Fee L, Grimsley G, & Gray T (1995) How to measure and predict the molar absorption coefficient of a protein. *Protein Sci.* 4:2411-2423.

13. Falk M (1964) Ultraviolet Spectra of Native + Denatured Deoxyribonucleic Acid. *J. Am. Chem. Soc.* 86(6):1226.

14. Antonini E & Brunori M (1971) *Hemoglobin and Myoglobin in Their Reactions With Ligands* (North-Holland Publishing Company, Amsterdam, London) p 44.

15. Schreckenbach T, Walckhoff B, & Oesterhelt D (1977) Studies on the retinal-protein interaction in bacteriorhodopsin. *Eur. J. Biochem.* 76:499–511.

16. Kelly SW, Jess TJ, & Price NC (2005) How to Study Protein by Circular Dichroism. *Biochim. Biophys. Acta* 1751:119-139.

17. Elöve GA, Chaffotte AF, Roder H, & Goldberg ME (1992) Early Steps in Cytochrome c Folding Probed by Time-Resolved Circular Dichroism and Fluorescence Spectroscopy. *Biochemistry* 31:6876-6883.

18. Jennings PA & Wright PE (1993) Formation of a Molten Globule Intermediate Early in the Kinetic Folding Pathway of Apomyoglobin. *Science* 262:892-896.

19. Kaltashov IA, Bobst CE, & Abzalimov RR (2013) Mass spectrometry-based methods to study protein architecture and dynamics. *Protein Sci.* 22(5):530-544.

20. Bruins AP, Covey TR, & Henion JD (1987) Ion Spray Interface for Combined Liquid Chromatography/Atmospheric Pressure Ionization Mass Spectrometry. *Anal. Chem.* 59:2642-2646.

21. Medzihradszky KF, Besman MJ, & Burlingame AL (1998) Reverse-phase Capillary High Performance Liquid Chromatography/High Performance Electrospray Ionization Mass Spectrometry: An Essential Tool for the Characterization of Complex Glycoprotein Digests. *Rapid Commun. Mass Spectrom.* 12:472-478.

22. Liu C & Verma SS (1999) Direct Coupling of Ionic High-Performance Liquid Chromatography with Electrospray Ionization Mass Spectrometry Utilizing a Microdialysis Junction Interface. *J. Chromatogr. A* 835:93-104.

23. Niessen WM (1999) State-of-the-Art in Liquid Chromatography-Mass Spectrometry. *J. Chromatogr. A* 856:179-197.

24. Fang L, *et al.* (2002) High-throughput liquid chromatography ultraviolet/mass spectrometric analysis of combinatorial libraries using an eight-channel multiplexed electrospray time-of-flight mass spectrometer. *Rapid Commun. Mass Spectrom.* 16:1440-1447.

25. Carbeck JD, *et al.* (1998) Correlation between the charge of proteins in solution and in the gas phase investigated by protein charge ladders, capillary electrophoresis, and electrospray ionization mass spectrometry. *J. Phys. Chem. B* 102(51):10596-10601.

26. Mittermaier A & Kay LE (2006) New Tools Provide New Insights in NMR Studies of Protein Dynamics. *Science* 312:224-228.

27. Parker MW (2003) Protein Structure from X-Ray Diffraction. *J. Biol. Phys.* 29:341-362.

28. Summerfield SG & Gaskell SJ (1997) Fragmentation efficiencies of peptide ions following low energy collisional activation. *Int. J. Mass Spectrom.* 165/166:509-521.

29. Heck AJR & Van den Heuvel RHH (2004) Investigation of intact protein complexes by mass spectrometry. *Mass Spectrom. Rev.* 23:368-389.

30. Fenn JB (2003) Electrospray Wings for Molecular Elephants (Nobel Lecture). *Angew. Chem. Int. Ed.* 42:3871-3894.

31. Tang L & Kebarle P (1993) Dependence of ion intensity in electrospray mass spectrometry on the concentration of the analytes in the electrosprayed solution. *Anal. Chem.* 65:3654-3668.

32. Kebarle P & Verkerk UH (2009) Electrospray: From Ions in Solutions to Ions in the Gas Phase, What We Know Now. *Mass Spectrom. Rev.* 28:898-917.

33. Taylor G (1954) Conditions under which dispersion of a solute in a stream of solvent can be used to measure molecular diffusion. *Proc. Roy. Soc. Lond. A* 225:473-477.

34. Yuill EM, Sa N, Ray SJ, Hieftje GM, & Baker LA (2013) Electrospray Ionization from Nanopipette Emitters with Tip Diameters of Less than 100 nm. *Anal. Chem.* 85(18):8498-8502.

35. Nguyen S & Fenn JB (2007) Gas-phase ions of solute species from charged droplets of solutions. *Proc. Natl. Acad. Sci. U.S.A.* 104:1111-1117.

36. Hogan CJ, Carroll JA, Rohrs HW, Biswas P, & Gross ML (2009) Combined Charged Residue-Field Emission Model of Macromolecular Electrospray Ionization. *Anal. Chem.* 81:369-377.

37. Konermann L, Ahadi E, Rodriguez AD, & Vahidi S (2013) Unraveling the Mechanism of Electrospray Ionization. *Anal. Chem.* 85:2-9.

38. Rayleigh L (1882) On the Equilibrium of Liquid Conducting Masses charged with Electricity. *Phil. Mag.* 14:184-186.

39. Kaltashov IA & Mohimen A (2005) Estimates of Protein Surface Area in Solution by Electrospray Ionization Mass Spectrometry. *Anal. Chem.* 77:5370-5379.

40. de la Mora FJ (2000) Electrospray Ionization of large multiply charged species proceeds via Dole's charged residue mechanism. *Anal. Chim. Acta* 406:93-104.

41. Konermann L, Rodriguez AD, & Liu J (2012) On the Formation of Highly Charged Gaseous Ions from Unfolded Proteins by Electrospray Ionization. *Anal. Chem.* 84:6798–6804.

42. Sciuto SV, Liu J, & Konermann L (2011) An Electrostatic Charge Partitioning Model for the Dissociation of Protein Complexes in the Gas Phase. *J. Am. Soc. Mass Spectrom.* 22:1679-1689.

43. Iribarne JV & Thomson BA (1976) On the evaporation of small ions from charged droplets. *J. Chem. Phys.* 64:2287-2294.

44. Karas M & Hillenkamp F (1988) Laser Desorption Ionization of Proteins with Molecular Masses Exceeding 10 000 Daltons. *Anal. Chem.* 60:2299-2301.

45. Douglas DJ, Frank AJ, & Mao D (2005) Linear Ion Traps in Mass Spectrometry. *Mass Spectrom. Rev.* 24:1-29.

46. Makarov A (2000) Electrostatic Axially Harmonic Orbital Trapping: A High-Performance Technique of Mass Analysis. *Anal. Chem.* 72:1156-1162.

47. Scigelova M & Makarov A (2006) Orbitrap Mass Analyzer - Overview and Applications in Proteomics. *Proteomics* 6 Suppl. 2:16-21.

48. Zubarev AR & Makarov A (2013) Orbitrap Mass Spectrometry. *Anal. Chem.* 85:5288-5296.

49. Marshall AG, Hendrickson CL, & Jackson GS (1998) Fourier Transform Ion Cyclotron Resonance Mass Spectrometry: A Primer. *Mass Spectrom. Rev.* 17:1-35.

50. Iribarne JV, Dziedzic PJ, & Thomson BA (1983) Atmospheric pressure ion evaporation - mass spectrometry. *Int. J. Mass. Spectrom.* 50:331-347.

51. Yamashita M & Fenn JB (1984) Electrospray Ion Source. Another variation on the Free-Jet Theme. *J. Phys. Chem.* 88:4451-4459.

52. Fenn JB, Mann M, Meng CK, Wong SF, & Whitehouse CM (1990) Electrospray ionization-principles and practice. *Mass Spectrom Rev.* 9:37-70.

53. Smith RD, Loo JA, Baringa CJ, Edmonds CG, & Udseth HR (1990) Collisional Activation and Collision-Activated Dissociation of Large Multiply Charged Polypeptides and Proteins Produced by Electrospray Ionization. *J. Am. Soc. Mass Spectrom.* 1:53-65.

54. Mirza UA, Cohen SL, & Chait BT (1993) Heat-Induced Conformational Changes in Proteins Studied by Electrospray Ionisation Mass Spectrometry. *Anal. Chem.* 65:1-6.

55. Verentchikov AN, Ens W, & Standing KG (1994) Reflecting Time-of-Flight Mass Spectrometer with an Electrospray Ion-Source and Orthogonal Extraction. *Anal. Chem.* 66(1):126-133.

56. Covey TR, Huang EC, & Henion JD (1991) Structural Characterization of Protein Peptides via Liquid Chromatography/Mass Spectrometry and Collision-Induced Dissociation of Their Doubly Charged Molecular Ions. *Anal. Chem.* 63:1193-1200.

57. Kruger NA, *et al.* (1999) Electron Capture versus energetic dissociation of protein ions. *Int. J. Mass Spectrom.* 182/183:1-5.

58. Kruger NA, Zubarev RA, Horn DM, & McLafferty FW (1999) Electron capture dissociation of multiply charged peptide cations. *Int. J. Mass Spectrom.* 185-187:787-793.

59. Zubarev RA, *et al.* (2000) Electron Capture Dissociation for Structural Characterization of Multiply Charged Protein Cations. *Anal. Chem.* 72:563-573.

60. McLafferty FW, *et al.* (2001) Electron Capture Dissociation of Gaseous Multiply Charged Ions by Fourier-Transform Ion Cyclotron Resonance. *J. Am. Soc. Mass Spectrom.* 12:245-249.

61. Syka JEP, Coon JJ, Schroeder MJ, Shabanowitz J, & Hunt DF (2004) Peptide and protein sequence analysis by electron transfer dissociation mass spectrometry. *Proc. Natl. Acad. Sci. U.S.A.* 101:9528-9533.

62. Molina H, Horn DM, Tang N, Mathivanan S, & Pandey A (2007) Global proteomic profiling of phosphopeptides using electron transfer dissociation tandem mass spectrometry. *Proc. Natl. Acad. Sci. U.S.A.* 104:2199-2204.

63. Abzalimov RR, Kaplan DA, Easterling ML, & Kaltashov IA (2009) Protein conformations can be probed in top-down HDX MS experiments utilizing electron transfer dissociation of protein ions without hydrogen scrambling. *J. Am. Soc. Mass Spectrom.* 20:1514-1517.

64. Rand KD, Zehl M, Jensen ON, & Jørgensen TJD (2009) Protein Hydrogen Exchange Measured at Single-Residue Resolution by Electron Transfer Dissociation Mass Spectrometry. *Anal. Chem.* 81:5577-5584.

65. Hunt DF, Yates III JR, Shabanowitz J, Winston S, & Hauer CR (1986) Protein sequencing by tandem mass spectrometry. *Proc. Natl. Acad. Sci. U.S.A.* 83:6233-6237.

66. Mueller DR, Eckersley M, & Richter WJ (1988) Hydrogen transfer reactions in the formation of "Y + 2" sequence ions from protonated peptides. *Org. Mass Spectrom.* 23:217-222.

67. Biemann K & Scoble HA (1987) Characterization by Tandem Mass Spectrometry of Structural Modifications in Proteins. *Science* 237:992-998.

68. Loo JA, Edmonds CG, & Smith RD (1991) Tandem Mass Spectrometry of Very Large Molecules: Serum Albumin Sequence Information from Multiply Charged Ions Formed by Electrospray Ionization. *Anal. Chem.* 63:2488-2499.

69. Tang XJ, Thibault P, & Boyd RK (1993) Fragmentation Reactions of Multilpy-Protonated Peptides and Implications for Sequencing by Tandem Mass-

Spectrometry With Low-Energy Collision-Induced Dissociation. *Analytical Chemistry* 65(20):2824-2834.

70. Zubarev RA, *et al.* (1998) Tandem Mass Spectrometry of Disulfide Bonded Proteins using Electron Capture Dissociation. *J. Am. Chem. Soc.*:(submitted).

71. Srikanth R, *et al.* (2007) Improved Sequencing of Oxidized Cysteine and Methionine Containing Peptides Using Electron Transfer Dissociation. *J. Am. Soc. Mass Spectrom.* 18:1499-1506.

72. Ahn J, Jung MC, Wyndham K, Yu YQ, & Engen JR (2012) Pepsin Immobilized on High-Strength Hybrid Particles for Continuous Flow Online Digestion at 10 000 psi. *Anal. Chem.* 84(16):7256-7262.

73. Jones LM, Zhang H, Vidavsky I, & Gross ML (2010) Online, High-Pressure Digestion System for Protein Characterization by Hydrogen/Deuterium Exchange and Mass Spectrometry. *Anal. Chem.* 82:1171-1174.

74. Zhang HM, *et al.* (2008) Enhanced Digestion Efficiency, Peptide Ionization Efficiency, and Sequence Resolution for Protein Hydrogen/Deuterium Exchange Monitored by Fourier Transform Ion Cyclotron Resonance Mass Spectrometry. *Anal. Chem.* 80:9034-9041.

75. Busby SA, Chalmers MJ, & Griffin PR (2007) Improving digestion efficiency under H/D exchange conditions with activated pepsinogen coupled columns. *Intl. J. Mass. Spectrom.* 259:130-139.

76. Bohrer BC, Merenbloom SI, Koeniger SL, Hilderbrand AE, & Clemmer DE (2008) Biomolecule Analysis by Ion Mobility Spectrometry. *Annu. Rev. Anal. Chem.* 1:293-327.

77. Englander SW, Bai LM, & Sosnick TR (1997) Hydrogen exchange: The modern legacy of Linderstrøm-Lang. *Protein Sci.* 6:1101-1109.

78. Molday RS, Englander SW, & Kallen RG (1972) Primary Structure Effects on Peptide Hydrogen Exchange. *Biochemistry* 11:150-158.

79. Hvidt A & Nielsen SO (1966) Hydrogen exchange in proteins. *Adv. Protein Chem.* 21:287-386.

80. Wand AJ, Roder H, & Englander SW (1986) Two-Dimension ^{1}H NMR studies of Cytochrome *c*: Hydrogen Exchange in the N-Terminal Helix. *Biochem* 25:1107-1114.

81. Smith DL, Deng Y, & Zhang Z (1997) Probing the Noncovalent Structure of Proteins by Amide Hydrogen Exchange Mass Spectrometry. *J. Mass Spectrom.* 32:135-146.

82. Konermann L, Tong X, & Pan Y (2008) Protein Structure and Dynamics Studied by Mass Spectrometry: H/D exchange, hydroxyl radical labeling, and related approaches. *J. Mass Spectrom.* 43:1021-1036.

83. Fang J, Rand KD, Beuning PJ, & Engen JR (2011) False EX1 signatures caused by sample carryover during HX MS analyses. *Int. J. Mass Spectrom.* 302:19-25.

84. Katta V & Chait BT (1993) Hydrogen/Deuterium Exchange Electrospray Ionisation Mass Spectrometry: A Method for Probing Protein Conformational Changes in Solution. *J. Am. Chem. Soc.* 115:6317-6321.

85. Katta V & Chait BT (1991) Conformational Changes in Proteins Probed by Hydrogen-exchange Electrospray-ionisation Mass Spectrometry. *Rapid Commun. Mass Spectrom.* 5:214-217.

86. Barrera NP & Robinson CV (2011) Advances in the Mass Spectrometry of Membrane Proteins: From Individual Proteins to Intact Complexes. *Annu. Rev. Biochem.* 80:247-271.

87. Pan Y, Piyadasa H, O'Neil JD, & Konermann L (2012) Conformational Dynamics of a Membrane Transport Protein Probed by H/D Exchange and Covalent Labeling: The Glycerol Facilitator. *J. Mol. Biol.* 416:400-413.

88. Milne JS, Mayne L, Roder H, Wand AJ, & Englander SW (1998) Determinants of protein hydrogen exchange studied in equine cytochrome c. *Protein Sci.* 7:739-745.

89. Iacob RE & Engen JR (2012) Hydrogen Exchange Mass Spectrometry: Are We Out of the Quicksand? *J. Am. Soc. Mass Spectrom.* 23:1003-1010.

90. Percy AJ, Rey M, Burns KM, & Schriemer DC (2012) Probing protein interactions with hydrogen/deuterium exchange and mass spectrometry-A review. *Anal. Chim. Acta* 721:7-21.

91. Konermann L, Pan J, & Liu Y (2011) Hydrogen Exchange Mass Spectrometry for Studying Protein Structure and Dynamics. *Chem. Soc. Rev.* 40:1224-1234.

92. Kaltashov IA, Bobst CE, Abzalimov RR, Berkowitz SA, & Houde D (2010) Conformation and Dynamics of Biopharmaceuticals: Transition of Mass Spectrometry-Based Tools from Academe to Industry. *J. Am. Soc. Mass Spectrom.* 21:323-337.

93. Skinner JJ, Lim WK, Bédard S, Black BE, & Englander SW (2012) Protein dynamics viewed by hydrogen exchange. *Protein Sci.* 21:996-1005.

94. Zhang Z & Smith DL (1993) Determination of amide hydrogen exchange by mass sectrometry: a new tool for protein structure elucidation. *Protein Sci.* 2:522-531.

95. Hamuro Y, Coales SJ, Molnar KS, Tuske SJ, & Morrow JA (2008) Specificity of immobilized porcine pepsin in H/D exchange compatible conditions. *Rapid Commun. Mass Spectrom.* 22:1041-1046.

96. Ahn J, Cao M-J, Yu YQ, & Engen JR (2013) Accessing the reproducibility and specificity of pepsin and other aspartic proteases. *BBA - Proteins Proteomics* 1834(6):1222-1229.

97. Zhang Z, Post CB, & Smith DL (1996) Amide Hydrogen Exchange Determined by Mass Spectrometry: Application to Rabbit Muscle Aldolase. *Biochemistry* 35:779-791.

98. Wales TE, Fadgen KE, Gerhardt GC, & Engen JR (2008) High-Speed and High-Resolution UPLC Separation at Zero Degree Celsius. *Anal. Chem.* 80:6815-6820.

99. Deng Y, Zhang Z, & Smith DL (1999) Comparison of Continuous and Pulsed Labeling Amide Hydrogen Exchange/Mass Spectrometry for Studies of Protein Dynamics. *J. Am. Soc. Mass Spectrom.* 10:675-684.

100. Khanal A, Pan Y, Brown LS, & Konermann L (2012) Pulsed hydrogen/deuterium exchange mass spectrometry for time-resolved membrane protein folding studies. *J. Mass Spectrom.* 47:1620-1626.

101. Zhang Y, *et al.* (2013) Pulsed hydrogen-deuterium exchange mass spectrometry probes conformational changes in amyloid beta (A beta) peptide aggregation. *Proc. Natl. Acad. Sci. U.S.A.* 110(36):14604-14609.

102. Konermann L, Pan Y, & Stocks BB (2011) Protein folding mechanisms studied by pulsed oxidative labeling and mass spectrometry. *Curr. Opin. Struct. Biol.* 21:634-640.

103. Olsen JV, Ong S, & Mann M (2004) Trypsin Cleaves Exlusively C-terminal to Arginine and Lysine Residues. *Mol. Cell. Proteomics* 3:608-614.

104. Lacerda CMR, Xin L, Rogers I, & Reardon KF (2008) Analysis of iTRAQ data using Mascot and Peaks quantification algorithms. *Briefings Funct. Genomics Proteomics* 7:119-126.

105. Chalmers MJ, Busby SA, Pascal BD, West GM, & Griffin PR (2011) Differential hydrogen/deuterium exchange mass spectrometry analysis of protein-Ligand interactions. *Exp. Rev. Proteomics* 8:43-59.

Chapter 2 – ATP-Induced Dimerization of the F_OF_1 ε Subunit from *Bacillus PS3*: A Hydrogen Exchange/Mass Spectrometry Study

2 Introduction

ATP synthase is the molecular machine responsible for the production of adenosine triphosphate from ADP and Pi (1-3). This multi-protein complex is associated with the plasma membrane of bacteria, the inner mitochondrial membrane, and the thylakoid membrane of chloroplasts (4). The proton-motive force (PMF) (5) that drives ATP synthesis is established by transmembrane proton translocation during respiration or photosynthesis. The overall architecture of ATP synthase is similar across the various kingdoms of life, with a membrane-embedded F_O and a cytosolic F_1 portion. F_O from bacteria exhibits the subunit stoichiometry ab_2c_n (with n = 10 for *E. coli*), and bacterial F_1 has the composition $(\alpha\beta)_3\gamma\delta\varepsilon$ (Figure 2.1a). Transmembrane proton flow causes rotation of the $c_n\gamma\varepsilon$ sub-complex. γ extends deep into the catalytic head, and its rotation triggers a series of conformational changes in $(\alpha\beta)_3$ that are coupled to the synthesis of three ATP molecules per revolution (6).

The conversion of electrochemical energy to mechanical energy, and ultimately to chemical energy represents the normal function of ATP synthase. However, the enzyme is also capable of operating in reverse (7). This ATPase activity can help the cell cope with a drop in PMF. Under such conditions ATP hydrolysis keeps the membrane energized, thereby maintaining the viability of processes such as ion transport and flagellar motion (8). This hydrolytic activity of F_OF_1 must be tightly regulated because a depletion of the cellular ATP pool can have catastrophic consequences for the cell. One regulatory mechanism in bacteria, plants, and mitochondria involves binding of MgADP (without Pi) to catalytic sites on $(\alpha\beta)_3$, resulting in deactivation of the complex (7, 9-11).

A second regulatory mechanism in bacterial F_OF_1 involves the ε subunit (12, 13). The role of ε appears to be twofold. During ATP synthesis ε is required for effective coupling (14, 15). On the other hand, ε represents an inhibitor of F_1-mediated ATP

hydrolysis (9, 11). ε is a ~15 kDa protein that can adopt at least two different conformations. Studies on isolated ε from *E. coli* (Eε) revealed a compact structure consisting of two domains (Figure 2.1b) (16, 17). The N-terminal part folds into a β sandwich that comprises ten strands. The C-terminal domain forms a helix-loop-helix motif. Contacts between these helices (α1 and α2) are mediated by interdigitation of Ala residues. Hydrophobic contacts are found at the interface of the two domains. A similar compact structure is seen for the mitochondrial homolog of ε ("δ") when it is bound to F_1 (18). Crosslinking (19) and crystallization studies (20, 21) provided initial evidence that Eε can also adopt a more extended structure. This has been confirmed by X-ray analysis of *E. coli* F_1 where the helix-loop-helix motif of Eε has opened up, such that α2 extends into the catalytic head where it interacts with γ and $(\alpha\beta)_3$ (Figure 2.1a,c) (14). It has been proposed that the compact state of Eε allows both ATP synthesis and hydrolysis to occur. The extended form may permit rotation in the synthesis direction only, while shutting down ATP hydrolysis (19). However, recent studies indicate that the mechanism of ε-mediated F_OF_1 inhibition is more complex than envisioned in this simple ratchet model (3, 7, 9, 14).

The switching state of ε within bacterial F_OF_1 depends on the PMF and on the torque applied to γ (14). The ε conformation is also affected by the presence of ATP (22). An ATP-binding site has been identified for ε from the thermophilic bacterium *Bacillus PS3* (Tε). ATP-bound isolated Tε crystallizes in the compact state (Figure 2.1d) (21). Other trinucleotides do not interact with the protein (23, 24). This specificity suggests that Tε may serve as an intracellular ATP level sensor (23, 24). Sequence analyses point to I(L)DXXRA as a conserved ATP-binding motif in many bacterial ε subunits (21). In the case of Tε this binding motif comprises residues D89 and R92. In addition, R99, R122, and R126 in helices α1 and α2 participate in the formation of a cationic pocket that accommodates the negatively charged triphosphate group of ATP (Figure 2.1d). The K_d value of the Tε-ATP interaction is in the sub-μM range at room temperature (25). Much lower affinities of 22 mM (21) and 2 mM (26) have been reported for isolated Eε, and for ε from *Bacillus subtilis*, respectively.

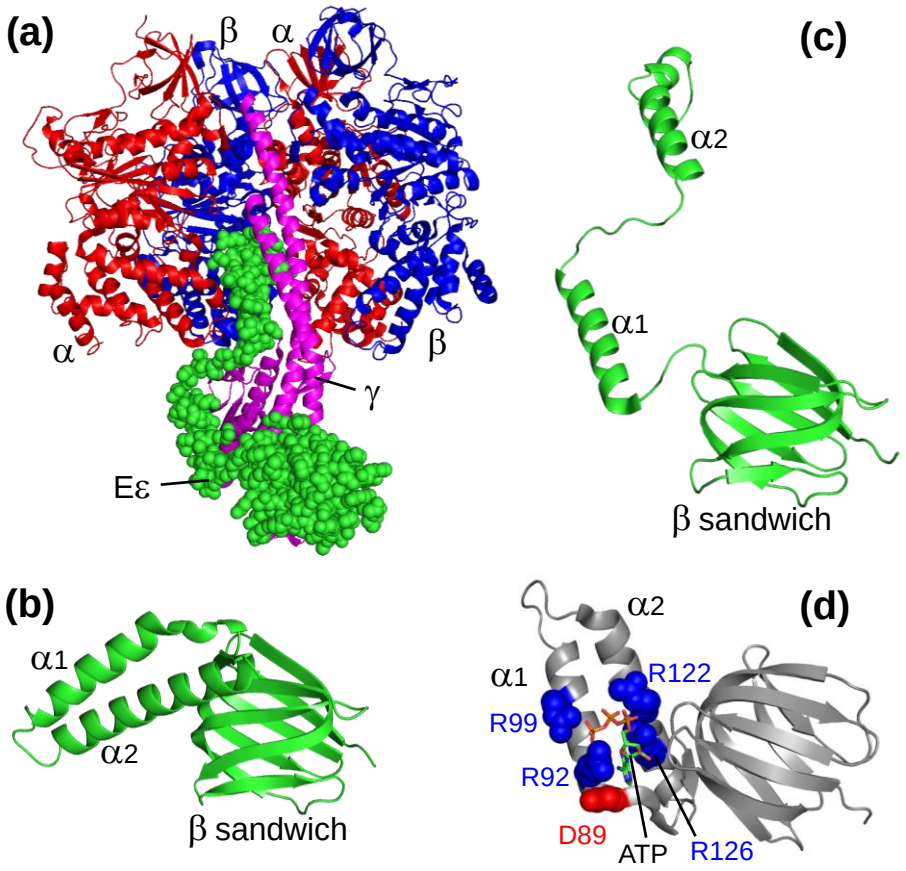

Figure 2.1 Crystal structure of F_1 and ε

(a) Crystal structure of the *E. coli* F_1 complex with subunits α (red), β (blue), γ (purple), and ε (referred to as Eε from now on, spacefill green). One αβ pair facing the observer has been omitted to provide a better view (PDB file 3OAA) (14). (b) Compact state of Eε, observed after crystallization of the isolated protein (PDB file 1AQT) (16). (c) Close-up of Eε in the extended conformation within the F_1 complex (from panel A). The orientation of the β sandwich in panels A-C is the same. (d) Crystal structure of ε from *Bacillus PS3* (referred to as Tε from now on) in the ATP-bound compact state (PDB file 2E5Y) (21). Key residues that interact with the ligand are shown in spacefill representation. The triphosphate group of ATP is depicted in red/orange. Note that the orientation of Eε and Tε in panels B, D is different.

Considering the wide range of ATP binding affinities for ε from different bacteria, the functional role of ε-ATP interactions remains yet to be fully explored (23). The ε subunit from chloroplasts does not possess an ATP binding site (27). It is also known that the mitochondrial homolog of ε is not involved in F_OF_1 inhibition; instead, the protein IF1 acts as inhibitor of ATPase activity in eukaryotes (28). This implies that bacterial ε represents an interesting antibiotic target (14, 29).

Considering the immense complexity of intact F_OF_1, a potential approach to understand the function of ε is via studies at the isolated protein level. Intriguingly, it has been demonstrated that ATP binding to isolated Tε induces major structural changes in the α1-α2 region (21, 24, 25). NMR experiments revealed that even truncated α1-α2 can bind ATP, forming a compact helix-loop-helix fold similar to that seen for ATP-bound Tε. Without ATP, truncated α1-α2 is more dynamic and the two helices are separated from each other, possibly resembling the inhibitory ε conformation seen in the crystal structure of intact F_OF_1 (Figure 2.1a) (14). Unfortunately, crystallographic data for ATP-free Tε are not available. Nonetheless, the findings of refs. (21, 25) suggest that functionally relevant ATP-induced switching may take place in isolated Tε, offering the opportunity to examine the switching mechanism by various biophysical techniques.

Hydrogen/deuterium exchange (HDX) coupled with mass spectrometry (MS) is a widely used method for probing protein structure, dynamics, and interactions (30-39). Solvent-exposed backbone N-H sites in unstructured regions exchange rapidly upon exposure to D_2O, with rate constants on the order of 1 s^{-1} (40). HDX at backbone sites that are involved in α-helices and β-sheets is much slower. Deuteration at these sites is mediated by conformational fluctuations that induce the transient opening of hydrogen bonds, coupled with exposure of N-H sites to the solvent. Thus, HDX in flexible regions proceeds much faster than in rigid segments. Ligand binding usually stabilizes the protein and induces a reduction in HDX rates. The largest changes tend to occur in regions that interact directly with the ligand, although allosteric effects can play a role as well (41, 42).

Here we employ HDX/MS in conjunction with circular dichroism (CD) spectroscopy and analytical ultracentrifugation (AUC) for studying the ATP-induced conformational switching of isolated Tε. We also examine the behavior of Eε for comparative purposes. ATP binding to Tε results in a highly unusual HDX protection pattern. With the aid of AUC experiments we demonstrate that this pattern originates from a previously unrecognized propensity of isolated Tε to dimerize in the presence of ATP.

2.1 Experimental

2.1.1 Materials

3-(N-morpholino)propanesulfonic acid (MOPS) was purchased from Fischer Scientific (Georgetown, ON), ATP was from MP Biomedicals (Santa Ana, CA). All purification steps were carried out at 4 °C, unless noted otherwise. Eε was expressed in in *E. coli* strain MM294 from plasmid pES2 (43) and purified by fractionation of cell extracts using ammonium sulfate precipitation followed by chromatography using Biogel HTP hydroxyapatite, DEAE-Sepharose, and Sephadex G-75 columns as described previously (44). Plasmid pTE2 encoding Tε was kindly provided by Prof. Yasuyuki Kato-Yamada (Department of Life Sciences, Rikkyo University, Japan) (45). It was expressed in *E. coli* strain BL21/DE3. Extracts of induced cells were fractionated by ammonium sulfate precipitation (45-65% of saturation), ion exchange chromatography at pH 8.0 on DEAE-Sepharose, and size exclusion chromatography on a Sephadex G75 column. Two peaks of pure Tε emerged from the G-75 column. Upon subsequent analysis on an Amersham Superdex 200 10/200 GL analytical size exclusion column run at 25 °C, the first peak eluted with a 260/280 absorbance ratio of 2.77, implying that it contained bound ATP, in agreement with previous findings (23). Similar analysis of the second peak gave a 260/280 absorbance ratio of 0.54 implying that it did not contain ATP. However, if a sample of the second peak was incubated with a 2-fold molar excess of ATP before application to the column, the protein eluted with a 260/280 ratio of 2.80,

indicating it was also capable of ATP binding. Tε for the experiments of this work were performed on protein from the first peak. ATP-free protein was generated from this stock by overnight dialysis at 20 °C in the presence of 15 U mL^{-1} yeast hexokinase against a solution containing 200 mM glucose as described (23). Hexokinase was subsequently separated from Tε by size exclusion chromatography on a preparative Sephadex G-75 column.

2.1.2 Hydrogen-Deuterium Exchange Mass Spectrometry

Ligand binding experiments were performed by initially pre-equilibrating 20 μM protein with either 1 mM (Tε) or 10 mM (Eε) ATP/$MgCl_2$ overnight in 25 mM MOPS-KOH (pH 7.0). Exchange was initiated by diluting the protein to 2 μM in deuterated buffer ($pH_{measured}$ = 7) at room temperature (22 ± 1 °C). 30 μL aliquots were taken at selected time points between 1 minute and 120 minutes, and quenched to pH 2.3 using buffer acidified with formic acid (FA). These aliquots were subsequently flash frozen in liquid N_2. For spatially resolved HDX/MS experiments the aliquots were rapidly thawed to ~0 °C and manually injected into a nanoACQUITY UPLC with HDX technology (Waters, Milford, MA) fitted with a POROS pepsin column (2.1 mm × 30 mm) from Life Technologies/Applied Biosystems (Carlsbad, CA). On-line pepsin digestion was conducted at 15 °C. Desalting and peptide separation were performed at 0 °C within 12 min on an equilibrated reversed phase column (BEH C18, 1.7 μm particle size, 1 mm × 100 mm) using a water/acetonitrile gradient with 0.1% FA at 40 μL min^{-1}. Fully deuterated controls (m_{100}) were employed to correct for back exchange. These controls were generated by protein incubation in exchange buffer at pH 2.0 for 24 h. Samples representing the t = 0 time point yielded the corresponding m_0 values. Biolynx 4.1 and DynamX (Waters) were used for data analysis. Deuteration levels (*%D*) were determined as

$$\%D = \left(\frac{m_t - m_0}{m_{100} - m_0} \right) \times 100\% \tag{2.1}$$

Experiments were performed on a Waters Synapt HDMS instrument equipped with a standard electrospray source that was operated at 2.8 kV. The source and desolvation temperatures were 80 and 300°C, respectively, and the cone voltage was 30 V. Peptide identification was performed using tandem mass spectrometry based on the known sequences of Eε and Tε (Figure S1).

2.1.3 Optical Measurements

CD spectra were recorded on a Jasco J-810 spectropolarimeter (Easton, MD) using a 1 mm cuvette at 25 °C . Blank spectra (25 mM MOPS-KOH pH 7.0) measured for protein-free solutions were subtracted from the CD data of 5 μM Tε and Eε measured in the presence and in the absence of 100 μM ATP. Experimental data were converted to mean residue ellipticity (θ). Analytical ultracentrifugation (AUC) experiments were performed at 20 °C on a Beckman XL-A instrument (Pasadena, CA) equipped with absorbance optics (46, 47). Tε samples were analyzed by sedimentation equilibrium measurements, with the buffer consisting of 25 mM MOPS-KOH (pH 7.0), 0.1 mM EDTA, with and without 25 mM ATP. Samples with protein concentrations of 33 μM were loaded into cells with six-channel Epon charcoal centerpieces and a 1.2 cm pathlength. These samples were initially sedimented at 20,000 rpm for 20 h to allow equilibration. Absorbance measurements at 280 nm were collected in 0.002 cm radial steps and averaged over 10 scans. Comparison with scans taken 4 hours earlier confirmed that equilibrium had been reached. Additional data sets were collected after subsequent equilibration at 25,000 and 30,000 rpm. All these data were globally fit using GraphPad Prism software according to the single-species model equation

$$C = C_0 \exp\left(\frac{\omega^2}{2RT} M_{obs}(1-\bar{v}\rho)(x^2 - x_0^2)\right) + I_0 \qquad (2.2)$$

where C is the concentration at radius x, C_o is the concentration at reference radius x_o, ω is the angular velocity of the rotor, $\bar{v}$ is the partial specific volume of the protein (calculated from its amino acid composition using the program SEDNTERP), ρ is the density of the solvent, R is the ideal gas constant, T is the absolute temperature, I_o is the

baseline offset, and M_{obs} is the measured molecular weight of the protein. AUC experiments conducted after addition of 100 mM KCl to the protein solutions yielded results that were identical to those shown below within experimental error. Reported M_{obs} values represent an average of triplicate measurements conducted at the three rotor speeds, for a total of nine runs for each condition.

2.2 Results and Discussion

2.2.1 Circular Dichroism

Eε exhibits a far-UV CD spectrum with a minimum around 220 nm, in accordance with earlier reports (48). These data are consistent with a mixed helical/sheet secondary structure (16). The addition of 100 μM ATP to Eε does not induce any significant spectral changes (Figure 2.2a). This finding is not surprising, considering the low ATP binding affinity of Eε (21), together with the known fact that Eε adopts a relatively well defined structure even in the absence of ATP (16, 17). CD measurements at higher ATP concentrations were precluded by the UV absorbance of the adenine moiety. A very different behavior is observed for Tε, where the addition of 100 μM ATP induces marked alterations in the CD spectrum (Figure 2.2b). The data acquired for ATP-bound Tε resembles resemble those of Eε in Figure 2A. In contrast, ATP-free Tε exhibits a reduced molar ellipticity around 222 nm, indicating a lower helicity (49). These observations are in line with the view that Tε possesses a high ATP binding affinity (25), and that ligand binding induces the formation of stable helical structure in the α1-α2 region (21). One factor that promotes the high ATP affinity of Tε is the accumulation of positive charges in the binding site (mainly due to Arg residues, Figure 2.1d), which mediate favorable electrostatic interactions with the triphosphate group. In the case of Eε this positive charge accumulation is less pronounced (21). Binding of ATP^{4-} to Tε in neutral solution may also be favored by bulk electrostatics, because Tε has a pI of 9.3, whereas that of Eε is 5.7.

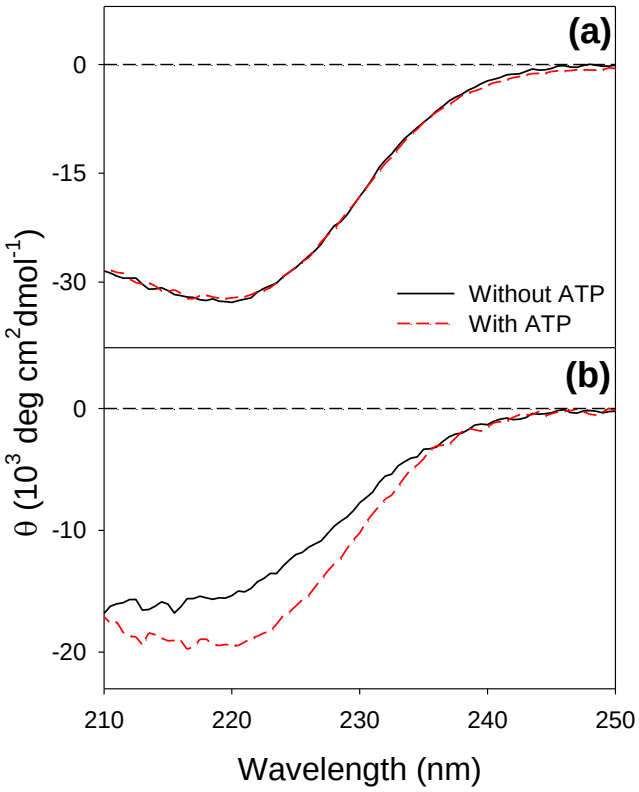

Figure 2.2 CD Analysis of Eε and Tε

Far-UV CD data of (a) Eε and (b) Tε in the absence (black) and presence (red) of 100 μM ATP. All other solution additives were as in the subsequent HDX experiments (except for the presence of D_2O).

2.2.2 Hydrogen-Deuterium Exchange Mass Spectrometry

Online peptic digestion of Eε and Tε yielded a large number of peptides. For each protein, 16 of these protein segments were selected that had sufficiently high S/N ratios for reliable HDX/MS measurements. The overall sequence coverage under these conditions was 99% and 86%, respectively, for Eε and Tε (Figure S1). HDX kinetics were measured with and without ATP to characterize ligand-induced changes in protein structure and dynamics. Initial experiments on Eε revealed that addition of 1 mM ATP did not cause any alterations compared to ATP-free samples (data not shown). The ATP concentration was then increased to 10 mM, which represents a typical intracellular value (50). However, even this elevated concentration did not induce any significant changes in the HDX behavior of Eε. As an example, unprocessed mass distributions for peptide 114-120 are depicted (Figure 2.3a-c). This is in contrast to the behavior of Tε, where dramatic differences in HDX kinetics were already observed after addition of 1 mM ATP (Figure 2.3d-f).

Deuterium uptake curves of the Eε and Tε peptides are depicted in Figures 2.4, 2.5. To better visualize these HDX data the peptide-resolved deuteration levels for t = 10 min were mapped onto the crystal structures of Eε and Tε (Figure 2.6). It is seen that in the absence of ATP the extent of deuteration tends to be higher for Tε than for Eε. The former shows almost complete deuteration throughout the entire protein sequence (Figure 2.6b), whereas Eε exhibits significant protection in the β sandwich, particularly the β8-β9 region (green, Figure 26a). Thus, in the absence of ATP the β sandwich region is more rigid in Eε than in Tε. Helices α1 and α2 appear to be quite dynamic for both proteins under these conditions. ATP binding induces a dramatic rigidification of Tε. The largest stabilizing effects are seen for β8-β9, as well as for α2 (blue, Figure 2.6c). Other Tε regions that become less dynamic upon ATP binding include parts of α1, as well as β1, β2, and β10 (green). The opposite site of the β sandwich retains high deuteration values after ATP binding (β3, β4, and β6; red/orange, Figure 2.6c). As noted earlier, no significant deuteration changes upon ATP addition are observed for Eε, and therefore only a single colored panel is shown for this protein (Figure 2.6a).

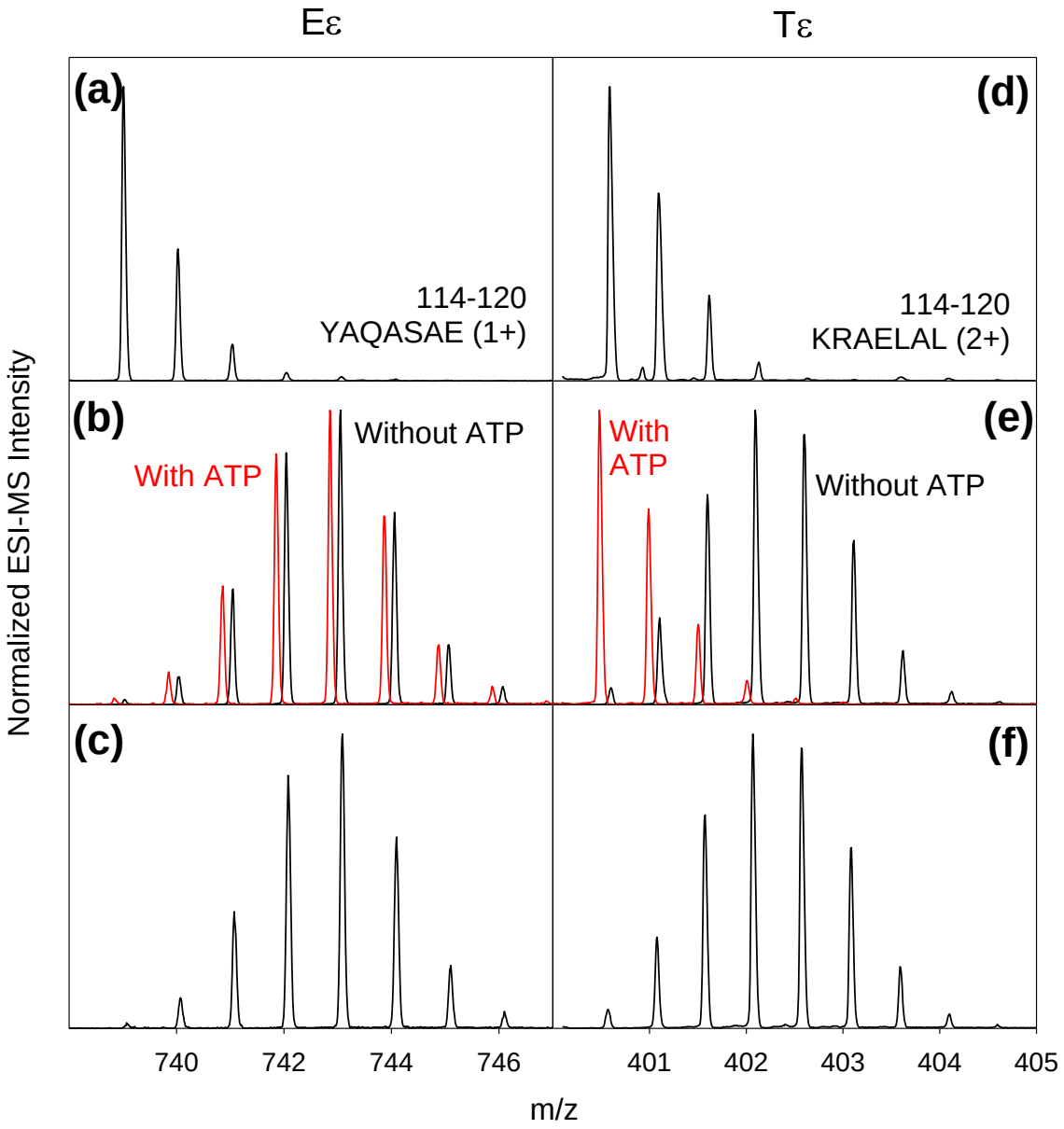

Figure 2.3 Unprocessed HDX-MS Data

Peptide 114-120 from Eε (a-c) and Tε (d-f). Spectra for unlabeled controls are shown in panels (a), (d). The corresponding data for the fully exchanged peptides are depicted in panels (c), (f). Panels (b), (e) show data acquired in the absence (black) and in the presence (red) of ATP for a labeling time of 10 minutes. The latter have been shifted in this Figure by -0.2 Da for better visualization.

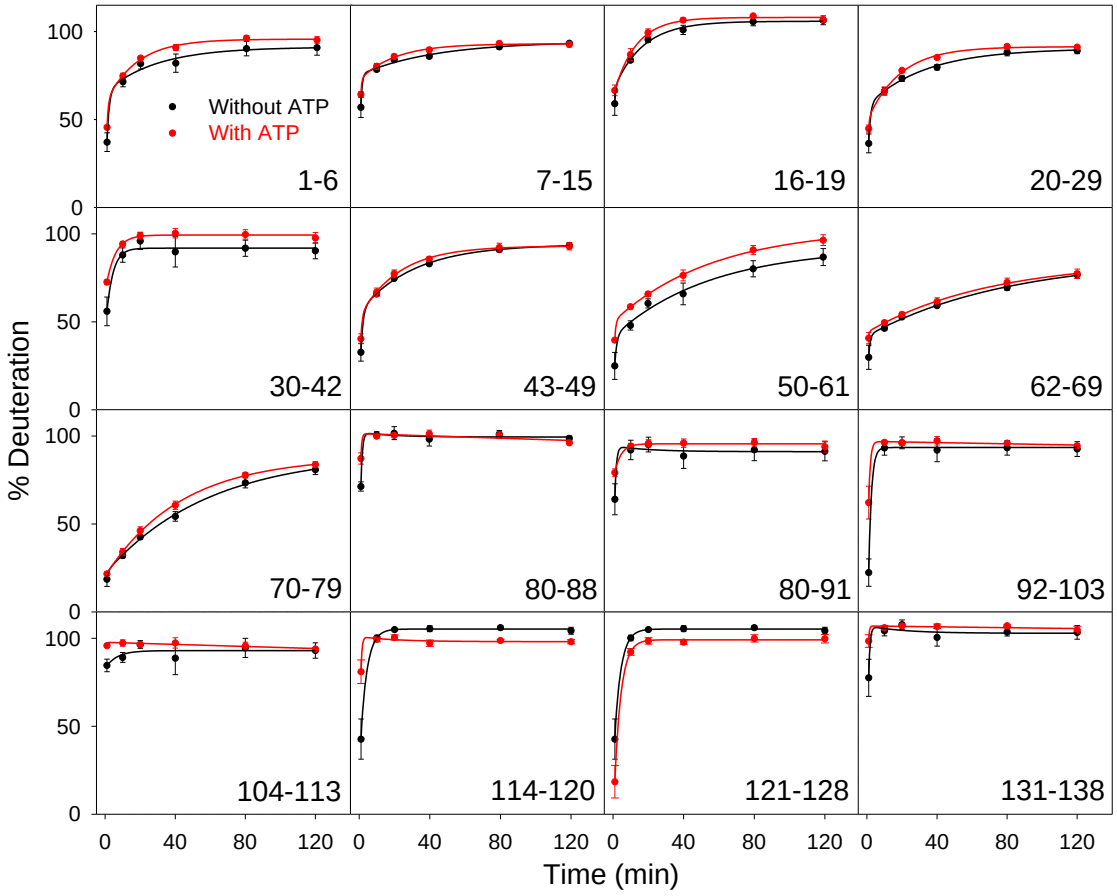

Figure 2.4 HDX kinetics of Eε peptides

HDX kinetics of Eε peptides in the absence (black) and presence (red) of 10 mM ATP. Residue numbers are indicated in each panel. Lines are biexponential fits. Error bars represent standard deviations of triplicate measurements.

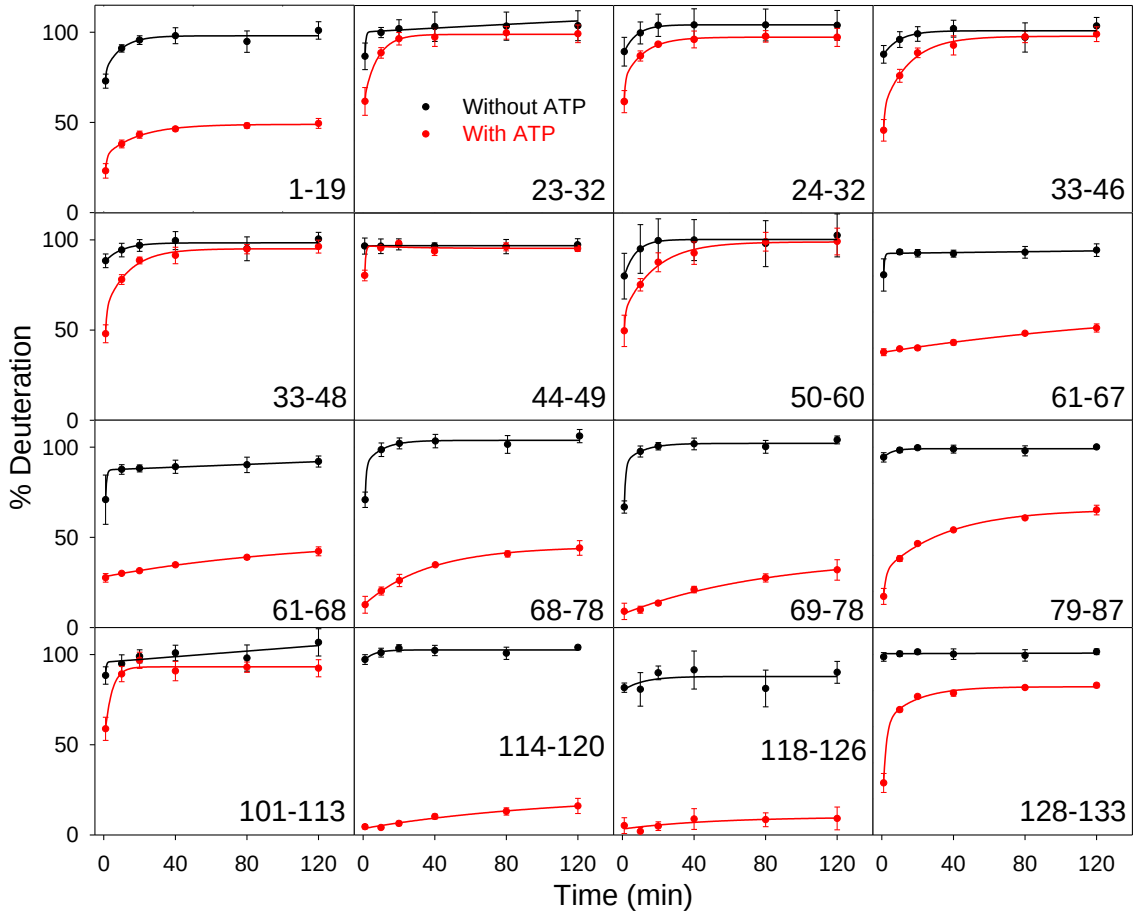

Figure 2.5 HDX kinetics of Tε peptides

HDX kinetics of Tε peptides in the absence (black) and presence (red) of 1 mM ATP. For additional information, see caption of Figure 2.4.

Previous room temperature studies on other systems have indicated reduced conformational dynamics for proteins from mesophilic organisms relative to their thermophilic homologues (51, 52). Cursory comparison of Eε and Tε in the absence of ATP seems to suggest that for the two proteins examined here this trend is reversed (Figure 2.6a, b). However, this type of comparison does not consider the ATP binding affinities of the two proteins which is in the sub-μM range for Tε (25), whereas Eε has a K_d that is two orders of magnitude higher (21). Under physiological conditions with [ATP] ≈ 10 mM(50) this implies that Tε will predominantly exist in the ATP-bound state, whereas Eε primarily remains ligand-free. In other words, a more pertinent way to compare the "physiologically relevant" state of the two proteins is to contrast Eε (Figure 2.6a) with ATP-bound Tε (Figure 2.6c). From this vantage point the mesophilic protein (Eε) is more dynamic than its thermophilic homolog (Tε), as previously reported for other proteins (51, 52).

2.2.3 ATP-Induced Dimerization of Tε

Protein-ligand interactions often lead to greatly reduced HDX rates in the vicinity of the binding site (53, 54). Based on the data presented so far, the stabilization of α2 upon ATP binding to Tε (Figure 2.6b, c) is consistent with such a local stabilizing effect. As noted, α2 comprises two of the residues that are directly involved in ATP binding (R122, and R126, Figure 2.1d). The β8-β9 segment is another area of Tε that undergoes a marked stabilization upon addition of ATP. This behavior is surprising, considering that β8-β9 is quite remote from the ATP binding site (Figure 2.6b, c). Allostery provides one possible explanation for such remote stabilization effects (41, 42); however, the subsequent considerations reveal that the β8-β9 protection has a different origin.

AUC experiments were conducted to gain additional insights into the properties of Tε in solution. In the absence of ATP the protein exhibits an M_{obs} of (17.7 ± 0.4) kDa, relatively close to the value of 14,562 Da that is expected on the basis of the amino acid sequence (Figure 2.7a). Surprisingly, addition of ATP resulted in a M_{obs} of (27.6 ± 0.3) kDa, i.e., almost twice the expected value (Figure 2.7b).

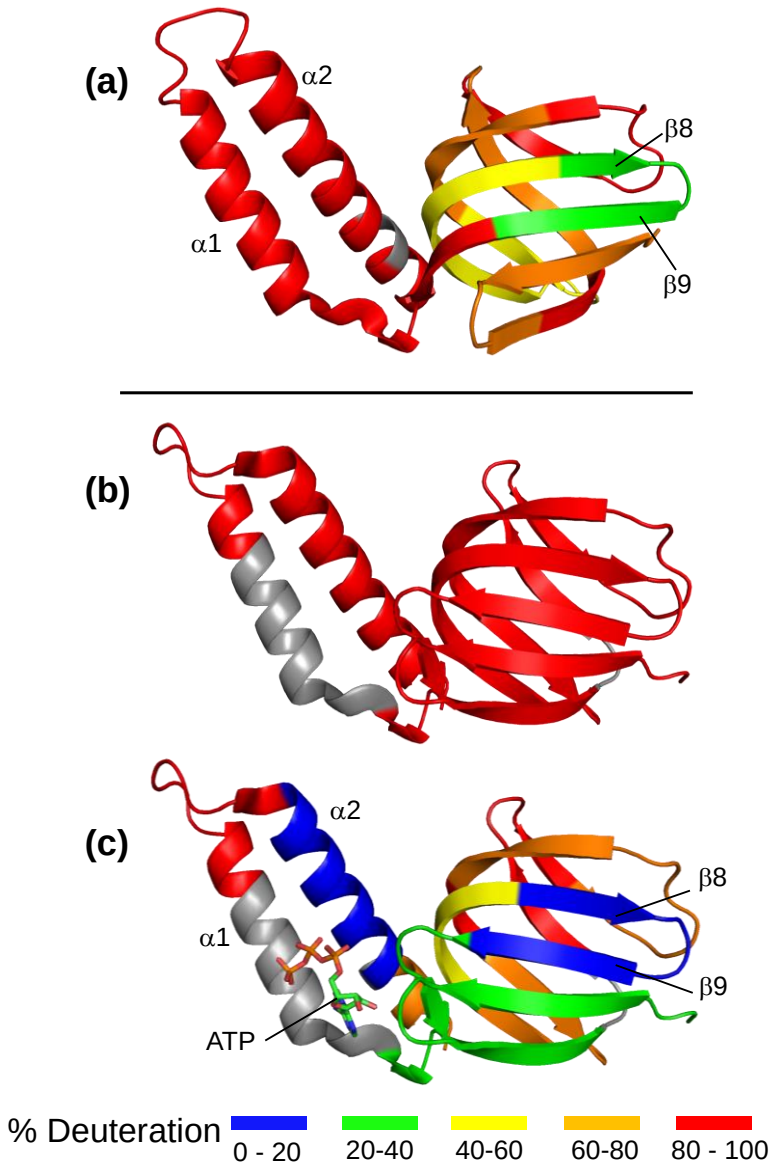

Figure 2.6 Crystal Structure Mapping of HDX Kinetics

(a) Mapping of the *t* = 10 min HDX data (from Figure 2.4) onto the X-ray structure of Eε. The corresponding HDX results for Tε (from Figure 2.5) in the absence and in the presence of ATP are shown in (b) and (c), respectively. Colors represent deuteration percentages as defined in the legend. Gray elements denote regions for which no suitable peptides were found after peptic digestion.

These results show that ATP-bound Tε forms a homodimer in solution. Analysis of the AUC data using a monomer-dimer model indicate that the protein-protein dissociation constant is in the range of 1 to 3 μM. To the best of our knowledge, the ATP-induced dimerization of Tε in solution has not been reported before. Earlier data on the solution-phase properties of this protein were interpreted with the implicit assumption of a monomeric state (21, 25).

Interestingly, X-ray crystallography provides direct evidence for the dimerization propensity of ATP-bound Tε. PDB file 2E5Y (21) shows the protein as a symmetric dimer, with one bound ATP molecule per subunit (Figure 2.8). Close interactions between the two chains exist in the β sandwich regions, particularly β8-β9 and β8'-β9'. These interactions are mediated by electrostatic contacts between the R71/E69/R71'/E69' side chains which adopt a tightly packed quadrupolar pattern. In addition, L78 and L78' are in hydrophobic contact with each other. The significant HDX protection of β8-β9 (and β8'-β9', blue in Figure 2.8) strongly suggests that these interchain contacts persist for ATP-bound Tε in solution. A second set of contacts is seen in the α1-α2 / α1'-α2' region, where the triphosphate of ATP interacts electrostatically with the K114' and R115' side chains from the *other* subunit (Figure 2.8). These favorable intermolecular charge-charge interactions are in addition to the contacts provided by R92, R99, R122, and R126 (Figure 2.1d). We conclude that the low deuteration values seen for α2 (and α2', blue in Figure 2.8) after ATP binding reflect the formation of both intra- and intermolecular contacts. Overall, our data demonstrate that the monomeric structure of Figure 1D does not adequately represent the ATP-bound state of Tε. Instead, the HDX protection pattern is consistent with the dimeric crystal structure of Figure 8 (21).

Readers might be surprised that the dimeric nature of ATP-bound Tε has thus far gone unrecognized, despite the fact that the protein crystallizes as a dimer. However, it can be difficult to extrapolate from the protein behavior in a crystal environment to the properties in solution. The most pertinent example in this context is Eε (1AQT) (16), which exhibits a crystal packing very similar to that of ATP-bound Tε (2E5Y) (21). Close β8-β9/β8'-β9' contacts are seen in both cases (16).

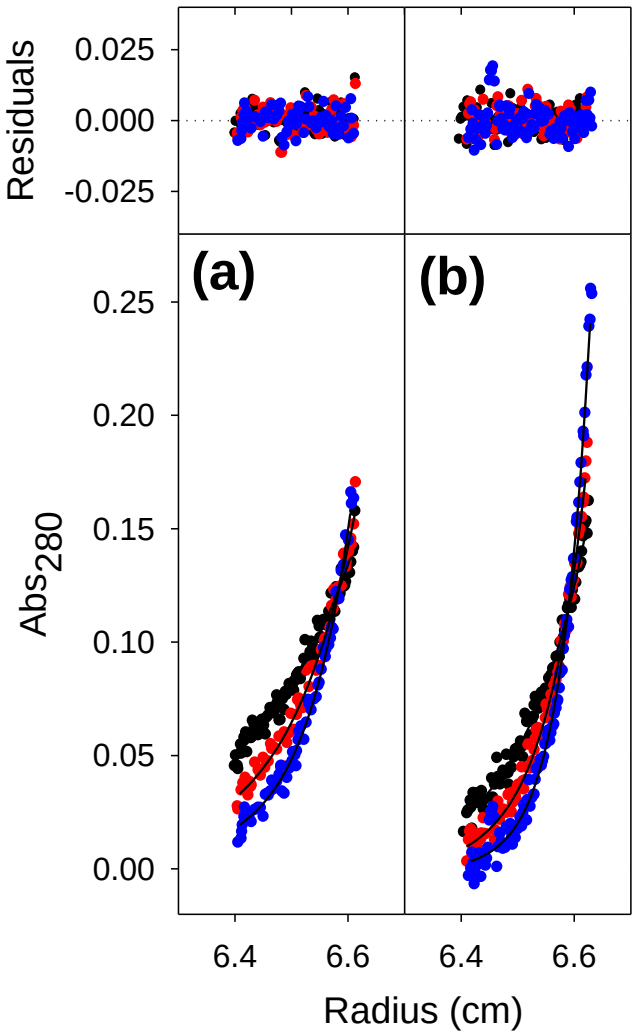

Figure 2.7 Sedimentation equilibrium AUC of Tε

Sedimentation equilibrium AUC runs of Tε in the absence (A) and presence (B) of ATP measured at rotor speeds of 20,000, 25,000, and 30,000 rpm (black, red and blue). Lines represent global fits according to Eq. 2.2.

Despite their similar X-ray structures, Eε is monomeric in solution (48) whereas the solution-phase state of ATP-bound Tε is a dimer (Figure 2.7). A difference between the β8-β9/β8'-β9' crystal contacts for Eε and Tε is that the former primarily involve hydrophobic interactions (16), whereas the latter have a strong electrostatic component (Figure 2.8). As an interesting side aspect we note that the β8-β9 surface also mediates binding between ε and γ in intact F_1 complexes (14, 16).

2.3 Conclusions

The key finding of this work is that isolated Tε undergoes dimerization upon ATP binding. ε (or its eukaryotic homolog "δ") represents a key component of the F_OF_1 machinery across all kingdoms of life. There is overwhelming evidence that ε (or "δ") functions as a monomeric subunit within F_OF_1 (14, 18, 20). It therefore is not immediately clear if the dimerization propensity uncovered here for isolated Tε has physiological relevance, although it clearly represents a feature that is interesting from a general protein chemistry perspective.

The inhibitory function of ε within F_OF_1 is linked to a conformational switch from an extended conformation to a more compact state (Figure 2.1a-c). In *Bacillus PS3* this transition can be triggered by ATP binding, such that the Tε may serve as an ATP level sensor (21). To obtain a better understanding of this switching event past studies (21, 25) followed an isolated-protein approach that assumed the net reaction

$$ATP + T\varepsilon_{extended} \rightarrow ATP\bullet T\varepsilon_{compact} \qquad (2.3)$$

It is not our intention to discredit those earlier experiments. However, the current work reveals an unexpected complication, *i.e.*, the fact that the actual conversion exhibited by isolated Tε involves dimerization according to

$$2\ ATP + 2\ T\varepsilon_{extended} \rightarrow (ATP\bullet T\varepsilon_{compact})_2 \qquad (2.4)$$

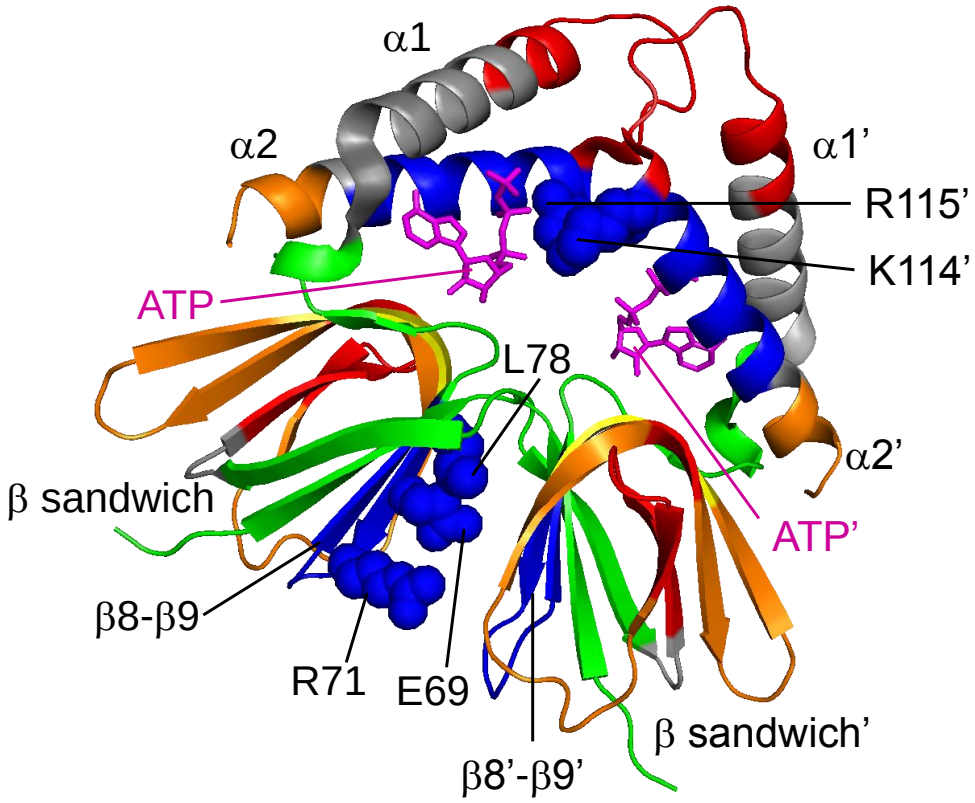

Figure 2.8 Dimerization of Tε

Crystal structure of ATP-bound dimeric Tε (2E5Y) (21). Colors indicate deuteration percentages for *t* = 10 min (from Figure 26c, where blue represents the lowest deuteration levels). Selected side chains and secondary structure elements of the complex are highlighted, using the absence or presence of a prime (‘) to differentiate between the two subunits. E69, R71, L78, K114, and R115 from each of the two chains form inter-subunit contacts. For each of the corresponding residue pairs only one member is highlighted to prevent cluttering.

The binding mode of ATP in the dimeric Tε complex comprises residues from *both* subunits, which is obviously different from the situation within F_OF_1 where only a single Tε subunit is present. In other words, mechanistic insights garnered from reaction (2.4) may not have direct implications for the regulatory function of Tε *in vivo*.

The fact that eukaryotes do not use ε for regulating their F_OF_1 activity highlights the potential of ε as an antibacterial target (14, 29). The findings reported here indicate a possible drug action mechanism involving the formation of tightly bound ε dimers in the presence of a high affinity ATP analog. The unique nature of the I(L)DXXRA binding motif on bacterial ε (21) implies that it might be feasible to develop specific high affinity ligands that do not interfere with the ATP metabolism of eukaryotes. Intercellular sequestration of bacterial ε in a dimeric form would limit the supply of free ε that is available for the assembly of functional F_OF_1, thereby slowing the growth of the pathogen without affecting the eukaryotic host. For assessing the feasibility of such an approach it will be necessary to conduct future studies on the ATP binding properties and dimerization propensities of ε from a wide range of bacteria.

2.4 References

1. Boyer PD (1997) The ATP Synthase - A Splendid Molecular Machine. *Annu. Rev. Biochem.* 66:717-749.

2. Stock D, Leslie AGW, & Walker JE (1999) Molecular Architecture of the Rotary Motor in ATP synthase. *Science* 286:1700-1705.

3. Borsch M & Duncan TM (2013) Spotlighting motors and controls of single FoF1-ATP synthase. *Biochem. Soc. Trans.* 41:1219-1226.

4. Schmidt C, *et al.* (2013) Comparative cross-linking and mass spectrometry of an intact F-type ATPase suggest a role for phosphorylation. *Nat. Commun.* 4:1-11.

5. Junge W, Sielaff H, & Engelbrecht S (2009) Torque generation and elastic power transmission in the rotary F0F1-ATPase. *Nature* 459(7245):364-370.

6. Wachter A, *et al.* (2011) Two rotary motors in F-ATP synthase are elastically coupled by a flexible rotor and a stiff stator stalk. *Proc. Natl. Acad. Sci. U. S. A.* 108(10):3924-3929.

7. Feniouk BA & Junge W (2005) Regulation of the F_0F_1-ATP synthase: The conformation of subunit ε might e determined by directionality of subunit γ rotation. *FEBS Lett.* 579:5114-5118.

8. Feniouk BA, Kato-Yamada Y, Yoshida M, & Suzuki T (2010) Conformational Transitions of Subunit ε in ATP Synthase from Thermophilic *Bacillus* PS3. *Biophys. J.* 98:434-442.

9. Shah NB, Hutcheon ML, Haarer BK, & Duncan TM (2013) The ε-inhibited state forms after ATP hydrolysis, is distinct fom the ADP-inhibited state, and responds dnamically to catalytic site ligands. *J. Biol. Chem.* 288(13):9383-9395.

10. Hirono-Hara Y, *et al.* (2001) Pause and rotation of F-1-ATPase during catalysis. *Proc. Natl. Acad. Sci. U. S. A.* 98(24):13649-13654.

11. Saita E, *et al.* (2010) Activation and Stiffness of the Inhibited States of F-1-ATPase Probed by Single-molecule Manipulation. *J. Biol. Chem.* 285(15):11411-11417.

12. Bulygin VV, Duncan TM, & Cross RL (1998) Rotation of the epsilon subunit during catalysis by Escherichia coli F0F1-ATP synthase. *J. Biol. Chem.* 273(48):31765-31769.

13. Kato-Yamada Y, Noji H, Yasuda R, Kinosita K, & Yoshida M (1998) Direct observation of the rotation of epsilon subunit in F-1-ATPase. *J. Biol. Chem.* 273(31):19375-19377.

14. Cingolani G & Duncan TM (2011) Structure of the ATP synthase catalytic complex (F_1) from *Escherichia coli* in an autoinhibited conformation. *Nat. Struct. Mol. Biol.* 18:701-708.

15. Cipriano DJ & Dunn SD (2006) The Role of the ε Subunit in the *Escherichia coli* ATP Synthase: The C-terminal Domain is Required for Efficient Energy Coupling. *J. Biol. Chem.* 281:501-507.

16. Uhlin U, Cox GB, & Guss JM (1997) Crystal structure of the ε subunit of the proton-translocating ATP synthase from *Escherichia coli*. *Structure* 5(9):1219-1230.

17. Wilkens S & Capaldi RA (1998) Solution structure of the epsilon subunit of the F-1-ATPase from Escherichia coli and interactions of this subunit with beta subunits in the complex. *J. Biol. Chem.* 273(41):26645-26651.

18. Gibbons C, Montgomery MG, Leslie AGW, & Walker JE (2000) The structure of the central stalk in bovine F-1-ATPase at 2.4 angstrom resolution. *Nat. Struct. Biol.* 7(11):1055-1061.

19. Tsunoda SP, *et al.* (2001) Large conformational changes of the ε subunit in the bacterial F_1F_0 ATP synthase provide a ratchet action to regulate this rotary motor enzyme. *Proc. Natl. Acad. Sci. U.S.A.* 98:6560-6564.

20. Rodgers AJW & Wilce MCJ (2000) Structure of the gamma-epsilon complex of ATP synthase. *Nat. Struct. Biol.* 7(11):1051-1054.

21. Yagi H, *et al.* (2007) Structures of the thermophilic F_1-ATPase ε subunit suggesting ATP-regulated arm motion of its C-terminal domain in F_1. *Proc. Natl. Acad. Sci. U.S.A.* 104:11233-11238.

22. Suzuki A, *et al.* (2003) F_0F_1-ATPase/Synthase is Geared to the Synthesis Mode by Conformational Rearrangement of ε Subunit in response to Proton Motive Force and ADP/ATP Balance. *J. Biol. Chem.* 278:46840-46846.

23. Kato-Yamada Y & Yoshida M (2003) Isolated ε Subunit of Thermophilic F_1-ATPase Binds ATP. *J. Biol. Chem.* 278:36013-36016.

24. Kadoya F, Kato S, Watanabe K, & Kato-Yamada Y (2011) ATP binding to the ε subunit of thermophilic ATP synthase is crucial for efficient coupling of ATPase and H^+ pump activities. *Biochem. J.* 437:135-140.

25. Iino R, *et al.* (2005) Real-time monitoring of conformational dynamics of the ε subunit in F_1-ATPase. *J. Biol. Chem.* 280(48):40130-40134.

26. Kato-Yamada Y (2005) Isolated ε subunit of *Bacillus subtilis* F_1-ATPase binds ATP. *FEBS Lett.* 579:6875-6878.

27. Yagi H, *et al.* (2010) Structural and functional analysis of the intrinsic inhibitor subunit ε of F_1-ATPase from photosynthetic organisms. *Biochem J.* 425:85-94.

28. Campanella M, Parker N, Tan CH, Hall AM, & Duchen MR (2009) IF1: setting the pace of the F1Fo-ATP synthase. *Trends Biochem. Sci.* 34(7):343-350.

29. Andries K, *et al.* (2005) A diarylquinoline drug active on the ATP synthase of Mycobacterium tuberculosis. *Science* 307(5707):223-227.

30. Konermann L, Pan J, & Liu Y (2011) Hydrogen Exchange Mass Spectrometry for Studying Protein Structure and Dynamics. *Chem. Soc. Rev.* 40:1224-1234.

31. Kaltashov IA, Bobst CE, & Abzalimov RR (2013) Mass spectrometry-based methods to study protein architecture and dynamics. *Protein Sci.* 22(5):530-544.

32. Iacob RE & Engen JR (2012) Hydrogen Exchange Mass Spectrometry: Are We Out of the Quicksand? *J. Am. Soc. Mass Spectrom.* 23:1003-1010.

33. Englander SW (2006) Hydrogen exchange and mass spectrometry: A historical perspective. *J. Am. Soc. Mass Spectrom.* 17(11):1481-1489.

34. Rob T, *et al.* (2012) Measuring Dynamics in Weakly Structured Regions of Proteins Using Microfluidics-Enabled Subsecond H/D Exchange Mass Spectrometry. *Anal. Chem.* 84:3771-3779.

35. Johnson RS & Walsh KA (1994) Mass spectrometric measurement of protein amide hydrogen exchange rates of apo- and holo-myoglobin. *Protein Sci.* 3:2411-2418.

36. Powell KD, *et al.* (2002) A General Mass Spectrometry-Based Assay for the Quantitation of Protein-Ligand Binding Interactions in Solution. *J. Am. Chem. Soc.* 124:10256-10257.

37. Zhu MM, Rempel DL, Du ZH, & Gross ML (2003) Quantification of protein-ligand interactions by mass spectrometry, titration, and H/D exchange: PLIMSTEX. *J. Am. Chem. Soc.* 125(18):5252-5253.

38. Asuru AP, An M, & Busenlehner LS (2012) Dissection of Porphyrin-Induced Conformational Dynamics in the Heme Biosynthesis Enzyme Ferrochelatase. *Biochemistry* 51(36):7116-7127.

39. Keppel TR, Howard BA, & Weis DD (2011) Mapping Unstructured Regions and Synergistic Folding in Intrinsically Disordered Proteins with Amide H/D Exchange Mass Spectrometry. *Biochemistry* 50(40):8722-8732.

40. Bai Y, Milne JS, Mayne L, & Englander SW (1993) Primary Structure Effects on Peptide Group Hydrogen Exchange. *Proteins: Struct., Funct., Genet.* 17:75-86.

41. Percy AJ, Rey M, Burns KM, & Schriemer DC (2012) Probing protein interactions with hydrogen/deuterium exchange and mass spectrometry-A review. *Anal. Chim. Acta* 721:7-21.

42. Chalmers MJ, Busby SA, Pascal BD, West GM, & Griffin PR (2011) Differential hydrogen/deuterium exchange mass spectrometry analysis of protein-Ligand interactions. *Exp. Rev. Proteomics* 8:43-59.

43. Skakoon EN & Dunn SD (1993) Location of Conserved Residue Histidine-38 of the ε Subunit of *Escherichia coli* ATP Synthase. *Arch. Biochem. Biophys.* 302:272-278.

44. Cipriano DJ & Dunn SD (2002) Genetic Fusions of Globular Proteins to the ε Subunit of the *Escherichia coli* ATP Synthase. *J. Biol. Chem.* 277:16782–16790.

45. Hara KY, Kato-Yamada Y, Kikuchi Y, Hisabori T, & Yoshida M (2001) The Role of the βDELSEED Motif of F_1-ATPase. *J. Biol. Chem.* 276: 23969 –23973.

46. Schuck P (2000) Size-Distrubution Analysis of Macromolecules by Sedimentation Velocity Ultracentrifugation and Lamm Equation Modeling. *Biophys. J.* 3:1606-1619.

47. Schuck P, Perugini MA, Gonzales NR, Howlett GJ, & Schubert D (2002) Size-Distrubution Analysis of Proteins by Analytical Ultracentrifugation: Strategies and Application to Model Systems. *Biophys. J.* 82:1096-1111.

48. Sternweis PC & Smith JB (1980) Characterization of the Inhibitory (Epsilon) Subunit of the Proton-Translocating Adenosine-Triphosphatase from *Escherichia-coli*. *Biochemistry* 19(3):526-531.

49. Kelly SW, Jess TJ, & Price NC (2005) How to Study Protein by Circular Dichroism. *Biochim. Biophys. Acta* 1751:119-139.

50. Beis I & Newsholme EA (1975) Contents of Adenine-Nucleotides, Phosphagens and some Glycolytic Intermediates in Resting Muscles from Vertebrates and Invertebrates. *Biochem. J.* 152(1):23-32.

51. Liang Z-X, Lee T, Resing KA, Ahn NG, & Klinman JP (2004) Thermal-activated protein mobility and its correlation with catalysis in thermophilic alcohol dehydrogenase. *Proc. Natl. Acad. Sci. U.S.A.* 101:9556-9561.

52. Wolf-Watz M, *et al.* (2004) Linkage between dynamics and catalysis in a thermophilic-mesophilic enzyme pair. *Nat. Struct. Mol. Biol.* 11(10):945-949.

53. Sperry JB, Smith CL, Caparon MG, Ellenberger T, & Gross ML (2011) Mapping the Protein–Protein Interface between a Toxin and Its Cognate Antitoxin from the Bacterial Pathogen Streptococcus pyogenes. *Biochemistry* 50:4038–4045.

54. Nakazawa S, Hashii N, Harazono A, & Kawasaki N (2012) Analysis of oligomeric stability of insulin analogs using hydrogen/deuterium exchange mass spectrometry. *Anal. Biochem.* 420:61-67.

Chapter 3 – HDX of a Redox-Active Proteins under Semi-Denaturing Conditions

3 Introduction

Redox-active proteins have been utilized extensively in literature to study various components of protein structure, function, and dynamics. Most redox-active proteins contain a signature prosthetic group, often a metal cation bound to a porphyrin cofactor. Some proteins are able to use these prosthetic groups to bind oxygen as in the case of myoglobin (1, 2), and hemoglobin (3-7). The absence of prosthetic groups can also affect protein folding, leading to the formation of molten-globule intermediates (8, 9).

One of the most commonly studied redox-active proteins is cytochrome *c* (Cyt *c*), a ~ 12.3 kDa protein containing the heme *c* moiety with an iron (Fe) center (10-17). The heme is covalently bound to the protein via two thioether linkages at positions Cys14 and Cys17 and is critical for proper folding (18). The Fe center is coordinated axially by the side chains of two amino acids, His18 and Met80 (Figure 3.1) (10)(11, 19, 20). Cyt *c* is found in the inner membrane of mitochondria and it does not bind oxygen. Instead, it is involved in the transport of electrons during cellular respiration. This is done *in vivo* by reducing the heme to Fe^{2+} (ferroCyt *c*) through the reaction of dihydroquinone (QH_2) and the cytochrome bc_1 complex. Cyt *c* is subsequently oxidized back to Fe^{3+} (ferriCyt *c*) via the cytochrome *c* oxidase complex (21-24). It is also possible to reduce the heme *in vitro* using a variety of reducing agents, with sodium dithionite (SDT) being the most commonly used. This reduction depends on the protein structure. The heme reduction potential in folded Cyt *c* is 260 mV vs. NHE (Normal Hydrogen Electrode) (25) and -100 mV for a heme in free solution (26, 27). If Cyt *c* is unfolded the reduction potential is closest that of free heme, therefore it is necessary to work with ferroCyt *c* under hypoxic conditions in order to prevent re-oxidation of the Fe center by atmospheric O_2 (28).

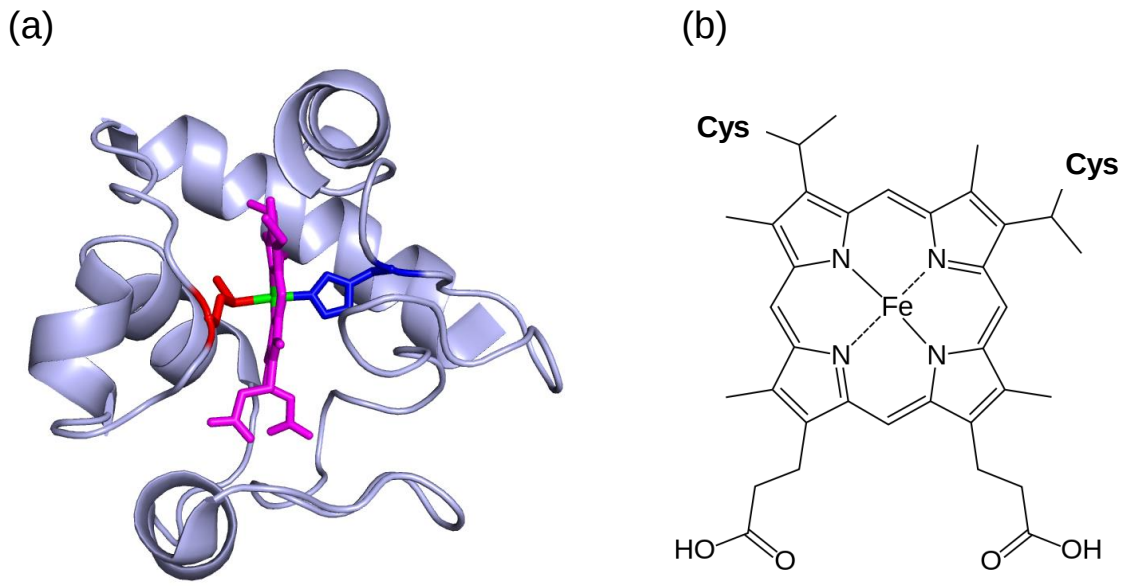

Figure 3.1 Cytochrome *c* structure.

(a) The structure of Cyt *c* (PDB file 1HRC) with the Fe center (green) of the heme (magenta) coordinated by His18 (blue) and Met80 (red). (b) The structure of heme *c* in Cyt *c*. The prosthetic group is bound via two thioether linkages at Cys14 and Cys17.

The structures of ferriCyt *c* and ferroCyt *c* are similar; however, they differ greatly in stability (18, 19). Equilibrium unfolding experiments with chemical denaturants (Urea or guanidinium hydrochloride, GdmHCl) have demonstrated that ferroCyt *c* is more stable than ferriCyt *c* (29-31). The reason for this stabilization is not obvious; however, it has been postulated that the higher charged Fe center of ferriCyt *c* can cause changes in protein solvation (32, 33). Electrostatic effects may also play a role in stabilization as the heme is electrically neutral in ferroCyt *c* and (+1) in ferriCyt *c*. HDX using MS (34) and 2D ^{1}H NMR (35) show a decrease in deuterium uptake upon reduction, however, localized changes in the protein were very minor. Considering the various techniques employed, a potential approach would be to combine individual methods together to study the structural differences in ferro/ferriCyt *c*. Denaturant-induced unfolding is useful in determining the degree in which a protein is destabilized, but, the destabilization cannot be localized to specific regions of the structure. HDX-MS has the potential to localize structural changes but this method *alone* is not able to determine the subtle changes in ferro/ferriCyt *c*. Therefore denaturant-induced unfolding to destabilize the protein structure, in conjunction with HDX-MS to monitor the degree of destabilization could be used to determine structural information the two techniques alone were unable to.

HDX kinetics of deuterium uptake relies on the opening/closing fluctuations of hydrogen bonding. These fluctuations are governed by the degree of secondary structure present in the protein. More importantly, the key to using HDX as a tool to study protein structure is that the protein, upon reaching equilibrium, does not undergo internal structural change. In the case of ferroCyt *c*, re-oxidation of the iron center by O_2 converts the protein to ferriCyt *c*. Because ferriCyt *c* is less stable, this would induce a shift in the protein equilibrium as the HDX is still in progress. It is unclear as to whether the protein can undergo sufficient HDX to elucidate structural information before the internal structure begins to change due to re-oxidation. This is because it is unknown as to how fast the re-oxidation occurs especially when denaturant, which destabilizes structure, is added. Therefore both the kinetic timeframe of re-oxidation and HDX must be compared to ensure HDX-MS is a valid method for studying the redox states of Cyt *c*.

Here we combine HDX-MS and denaturant-induced unfolding to examine ferroCyt *c* in order to garner information regarding structural stabilization. Cyt *c* is reduced using SDT and subject to HDX at increasing increments of GdmHCl, with the corresponding mass shift monitored by MS. In order to minimize re-oxidation due to the presence of O_2 both the reduction and HDX were done under stream of N_2. Similar experiments were performed on ferriCyt *c* as a control for re-oxidation. Very minute changes were observed with respect to the deuteration of ferroCyt *c* across increasing [GdmHCl] indicating the increased stability seen in literature. This coincides with larger increases observed in deuterium uptake under similar conditions with respect to the less stable ferroCyt *c*. Spectroscopic analysis reveal the re-oxidation kinetics to be faster than the HDX time course used, even at low [GdmHCl]. It is therefore unclear as to whether the HDX kinetics is truly based on a *homogenous* ferroCyt *c* population.

3.1 Experimental

3.1.1 Materials

Horse heart Cyt *c*, SDT, sodium phosphate (Na_2HPO4 and NaH_2PO_4), and sodium chloride (NaCl) were purchased from Sigma (St. Louis, MO). GdmHCl was purchased from Fischer Scientific (Georgetown, ON). D_2O was purchased from Cambridge Isotope Laboratories (Andover, MA). All chemicals were used as received. The buffer used in all experiments was 25 mM sodium phosphate (pH 7.0) with D_2O used in preparation instead of H_20 where appropriate.

3.1.2 Reduction of ferroCyt c

Prior to HDX ferroCyt *c* was treated with 30 fold excess of $Na_2S_2O_4$ to ensure the Fe center remained in the (+2) state. N_2 was passed over the buffer solution prior to addition of protein and maintained over the pre-exchange solution to remove O_2. NaCl was substituted for studies with ferriCyt *c* to ensure there were no discrepancies in ionic strength.

3.1.3 Intact HDX

Experiments were done by diluting the protein to a final concentration of 6 μM with deuterated buffer containing the desired concentration of GdmHCl (pH 7, 25°C). The final deuterium content of the exchange solution was 90% by volume. 60 μL aliquots were taken at selected time points and quenched to pH 2.3 using buffer acidified with formic acid (FA). The aliquot was subsequently flash frozen with $N_{2(l)}$ to halt deuterium exchange. The proteins were thawed and directed to the MS using a manual injection valve. Separation was done using a BEH300 C4 1.7μM 2.1 x 50mm column (Waters, Milford, MA) coupled to a UPLC pump (Waters) using an acidified water/acetonitrile gradient (0.1%FA) at 200 $\mu L min^{-1}$. The entire system including the column and solvent delivery lines were kept at 0°C. Deuteration levels (%D) were determined as:

$$\%D = \left(\frac{m_t - m_0}{m_{100} - m_0}\right) * 100 \tag{3.1}$$

%D was normalized and corrected for back-exchange using m_0, the mass of the undeuterated protein and $m_{100,}$ the mass of the fully deuterated protein. These values were calculated by measuring the mass of ferriCyt *c* with undeuterated buffer (m_0) and with exchange buffer at pH 2.0 for 24 h (m_{100})

3.1.4 ESI Mass Spectrometry

Experiments were performed on a Waters Synapt HDMS instrument using a source and desolvation temperature of 80 and 300°C, cone voltage of 30V, capillary voltage of 2.8 kV. A higher desolvation gas flow of 800 Lhr^{-1} was used to ensure the presence of high salt concentrations did not impair protein analysis.

3.1.5 Optical Measurements

UV-VIS spectra were recording on a Varian Cary 100 UV-visible spectrophotometer (Palto, Alto, CA) using 1 cm quartz cuvettes. Blank spectra containing phosphate and either $Na_2S_2O_4$/NaCl were used as a background correction. In order to profile the global structure of both ferro/ferriCyt *c* samples were pre-equilibrated for 1hr

with addition of GdmHCl up to 5.7M and subsequently analyzed. A scanning kinetics analysis was used to measure the absorbance of ferroCyt *c* as HDX every 10 min for 2 hr, the duration of a typical experiment.

3.2 Results and Discussion

3.2.1 Re-oxidation of ferroCyt c

To determine the extent of re-oxidation caused by denaturant-induced destabilization, UV spectra of both ferriCyt *c* and ferroCyt *c* were recorded under increasing [GdmHCl]. Native ferriCyt *c* exhibits an absorption maximum at 410 nm which is in agreement with previous literature (11). Upon denaturation the magnitude of the absorption increases as the Soret peak blue-shifts to 402 nm (Figure 3.2a). This increase in absorption is also observed in acid-unfolded ferriCyt *c* (11). Native ferroCyt *c* exhibits three characteristic absorption maxima at 550 (α), 520 (β) and 415 nm (γ). However upon unfolding, the α and β peak disappear with the overall spectra resembling that of ferriCyt *c* (Figure 3.2b). This is indicative of re-oxidation, facilitated by the presence of GdmHCl as an unfolding agent (36). Under native conditions the heme is sequestered within Cyt *c*, limiting solvent accessibility. Therefore the heme binding pocket must be pried open enough for oxygen to gain access for re-oxidation to occur. The presence of GdmHCl unfolds the protein exposing the pocket to the solvent and the dissolved O_2. The ligands around the Fe center also change upon unfolding, with the Met80 most likely being removed. His18 remains co-ordinated to the Fe center due to the preceding amino acid (Cys17) being covalently bound to the heme. The empty co-ordination site on the heme has been shown to enable carbon monoxide (CO) binding to ferroCyt *c* (28). Though Cyt *c* cannot bind O_2, this vacancy may allow for the appropriate redox reactions between oxygen and the Fe center to take place.

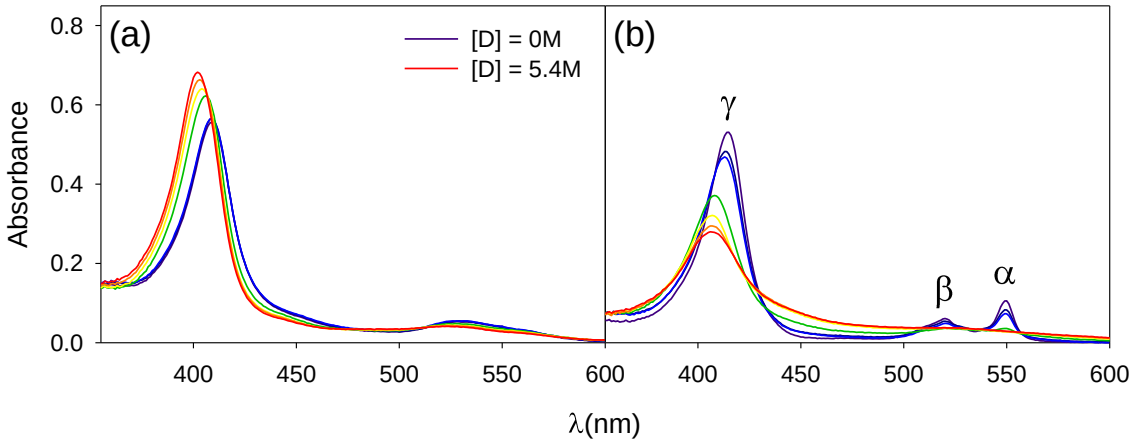

Figure 3.2 UV-VIS monitoring of ferro/ferriCyt *c* unfolding.

UV-VIS spectra corresponding to increases in 0.9 M GdmHCl increments for (a) ferriCyt *c* and (b) ferroCyt *c* are shown. The α and β peak diminishes at higher [D] conditions resembling panel A, indicating re-oxidation. Measurements were taken after samples were equilibrated for 1hr.

It is important to note that though there is excess $Na_2S_2O_4$ present to ensure the protein remains reduced, the opening of the heme pocket decreases the reduction potential of the heme itself. Therefore upon complete unfolding where the reduction potential is -100 mV, $Na_2S_2O_4$ can no longer keep the Fe center reduced.

UV-VIS spectra of ferroCyt *c* recorded during HDX reveal that the protein is in fact being slowly re-oxidized (Fig 3.3). This is evident from the absorbance decrease at 550nm corresponding to the α peak of native ferroCyt *c* (Fig 3.2b). The α peak is a good indicator for monitoring re-oxidation because it is characteristic to only ferroCyt *c*. Even in the absence of denaturant the re-oxidation process occurs slowly, on the order of 10% after 2hr. At 1.4 M GdmHCl the re-oxidation is more pronounced, therefore HDX studies at higher denaturant concentrations were not performed. The extent of re-oxidation cannot be determined under the current conditions; however, it can be estimated by examining native and unfolded Cyt *c* under true hypoxic conditions (28). Even unfolded ferroCyt *c* exhibits the characteristic α peak observed, provided the oxygen-free environment is maintained. Furthermore, the absorbance of the α peak decreases upon unfolding and is redshifted to 553 nm. Because λ_{max} does not change in the spectra of ferroCyt *c* under the present conditions, it is unlikely that the reduced form is being maintained. However, the subsequent HDX kinetics reveals a contrasting result to the spectroscopic analysis of ferroCyt *c* re-oxidation.

3.2.2 Intact HDX Analysis

The HDX kinetics of both ferriCyt *c* and ferroCyt *c* in the absence of denaturant were in general agreement with previous studies done, whereby reduced deuterium uptake was observed in ferroCyt *c* (Figure 3.4a) (34). Because the difference in *%D* is so small between the reduced and oxidized state, spatially resolved HDX-MS was not performed as it would be difficult to observe localized changes in deuterium uptake. This type of analysis was done previously, however the majority of the peptides did not demonstrate any changes (34). Two peptides (38-46, and 66-82 containing the heme ligand Met80) showed very small changes in deuterium uptake, on the order of 2-3 deuterons without back-exchange correction.

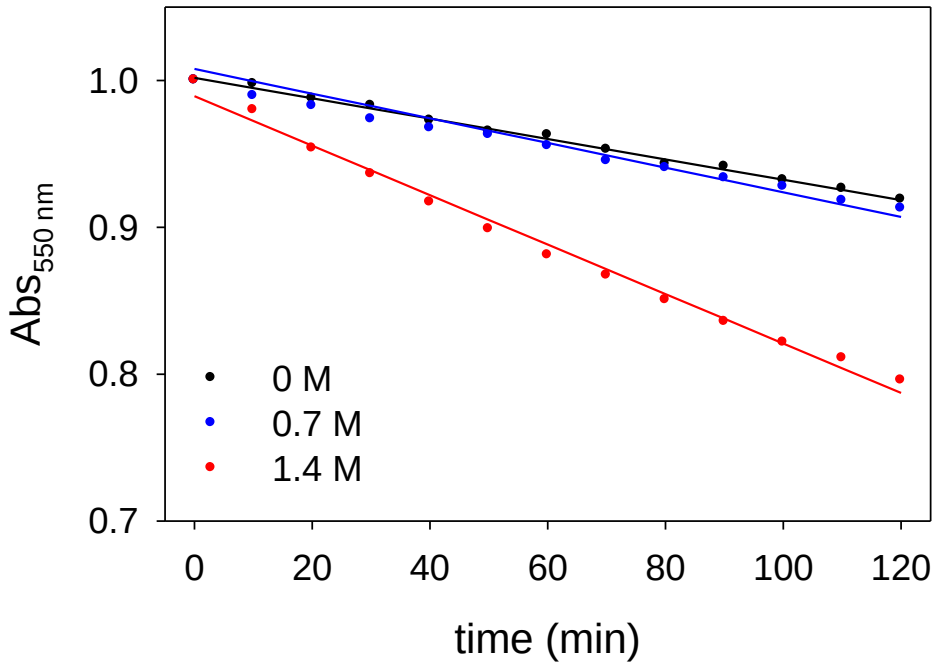

Figure 3.3 Monitoring re-oxidation of ferroCyt *c* during HDX

HDX exchange solutions were monitored by probing changes in the absorbance at 450 nm for 0.0M (black), 0.7M (blue) and 1.4M (red) GdmHCl.

In order to increase the difference in *%D*, the exchange was done using increasing [GdmHCl] (Figure 3.4b, c). There is a steady progression in HDX kinetics for ferriCyt *c*. This is most likely due to the increasing potency of GdmHCl destabilization, as secondary structure elements are more severely perturbed allowing for faster exchange. This progression is much less pronounced in the kinetics of ferroCyt *c*. It can be inferred that the secondary structure of ferroCyt *c* remains relatively unchanged as the denaturant concentration is increased. This suggests re-oxidation is not occurring because the heme pocket is not perturbed enough to allow O_2 to access the Fe center. Therefore the opening events of the binding pocket that cause re-oxidation are minimized due to the structural stability of ferroCyt *c*. If re-oxidation were occurring the HDX kinetics of ferroCyt c would begin to resemble the kinetics of ferriCyt *c*, which is not the case. However, taking into account the re-oxidation observed with optical measurements within the HDX time frame, the HDX kinetics are in fact more complex than initially thought.

It is intriguing that HDX and spectroscopic analyses present contrasting results. In terms of the HDX, the kinetics of ferroCyt *c* is different from that of ferriCyt *c*. More importantly the magnitude of this difference persists and somewhat increases upon denaturant addition (Fig 3.5). If the difference was to decrease and the kinetics of ferroCyt *c* began to resemble that of ferriCyt *c*, then it would most likely indicate re-oxidation or complete unfolding of the protein. This, however, is not the case and based on the HDX kinetics presented it seems that ferroCyt *c does not* re-oxidize. However spectroscopic data imply that ferroCyt *c does* re-oxidize during HDX studies, therefore the presence of a homogenous ferroCyt *c* population during HDX is less convincing. If the protein is in fact re-oxidizing it is puzzling as to why the HDX kinetics remain relatively unaltered as denaturant is added. At this stage of the research the current hypothesis is that the opening of the heme pocket does not trigger a substantial change in secondary structure. Without an appreciable change in the secondary structure, using HDX would prove difficult as it relies heavily on the presence of hydrogen bonding.

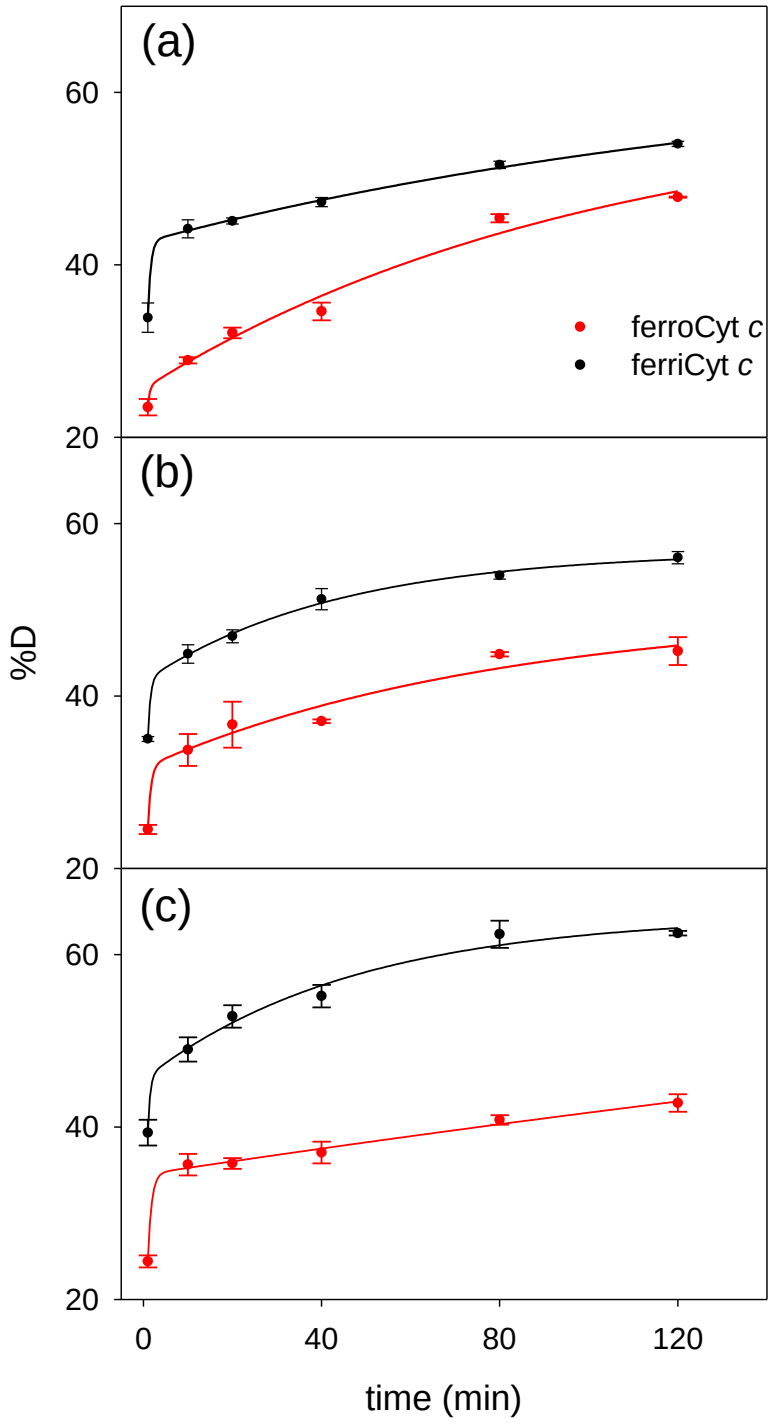

Figure 3.4 Intact HDX of ferro/ferriCyt *c*.

HDX kinetics of ferriCyt *c* (black) and ferroCyt *c* (red) for (a) 0.0 M (B) 0.7 M and (c) 1.4 M GdmHCl are shown.

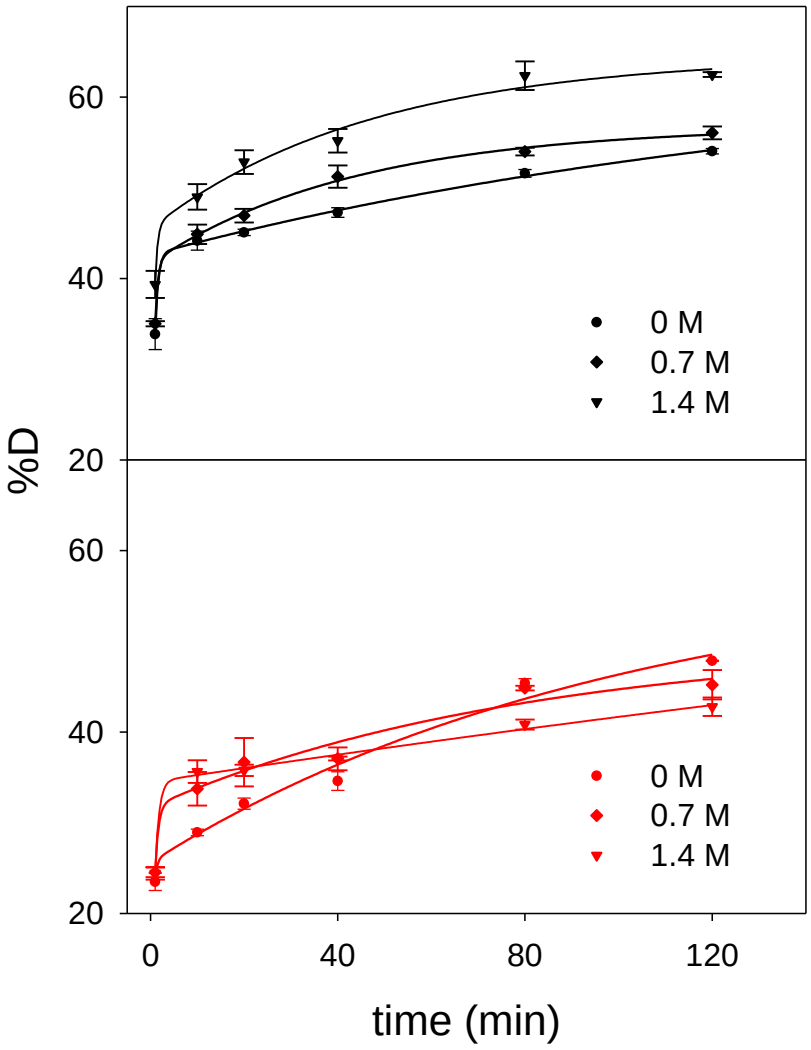

Figure 3.5 *%D* of ferro/ferriCyt *c* as a function of [GdmHCl].

Deuterium uptake of ferriCyt *c* at different *[D]*. (b) FerriCyt *c* does not demonstrate the same progression as in (a) signifying the increased stability due to the presence of a reduced heme center.

This matter is further complicated with the presence of GdmHCl. It is has been shown that using urea as a denaturant reduces HDX because urea interferes with hydrogen bonding, acting as a stand-in hydrogen bond acceptor (37). It remains unclear as to how GdmHCl affects protein structure especially in the case of HDX. Further work on the combined usage of HDX-MS and denaturant-induced unfolding is required to refine the technique in order to use it to study protein structure.

3.3 Conclusions

Monitoring the HDX kinetics of the ferri/ferroCyt *c* has demonstrated complications for the use of HDX-MS as a tool for studying protein structure. While it should be possible to generate truly oxygen-free conditions through means such as degassed solvents or a glove box, the difficulty of HDX-MS experiments under such conditions increases dramatically. This approach would still not guarantee a hypoxic environment because UPLC-MS instrumentation cannot reliably be purged of O_2. Therefore, at least in the context of the presented research it is not possible to distinguish between HDX kinetics caused by D_2O exposure and internal conversion to the oxidized state.

Due to time constraints further work must be done to complete this current aspect of research. Though the HDX could not be resolved based on underlying factors affecting deuterium uptake, the system demonstrated has the potential to correlate HDX kinetics with subtle structural dynamics, provided the structural change is irreversible. The HDX-MS analysis of Cyt *c* could be extended to ligand binding studies using carbon monoxide and cyanide. The rate at which HDX can occur under these conditions is dependent on the kinetics of ligand binding.

3.4 References

1. Li Y-T, Hsieh Y-L, Henion JD, & Ganem B (1993) Studies on Heme Binding in Myoglobin, Hemoglobin, and Cytochrome c by Ion Spray Mass Spectrometry. *J. Am. Soc. Mass Spectrom.* 4:631-637.

2. Evans SV & Brayer GD (1990) High-resolution Study of the Three-dimensional Structure of Horse Heart Metmyoglobin. *J. Mol. Biol.* 213:885-897.

3. Eaton WA, Henry ER, Hofrichter J, & Mozzarelli A (1999) Is cooperative oxygen binding by hemoglobin really understood. *Nat. Struct. Biol.* 6(4):351 - 358.

4. Bellelli A & Brunori M (2011) Hemoglobin allostery: Variations on the theme. *Biochim. Biophys. Acta* 1807(10):1262-1272.

5. Perutz MF, Wilkinson AJ, Paoli M, & Dodson GG (1998) The stereochemical mechanism of the cooperative effects in hemoglobin revisited. *Annu. Rev. Biophys. Biomolec. Struct.* 27:1-34.

6. Yonetani T & Laberge M (2008) Protein dynamics explain the allosteric behaviors of hemoglobin. *Biochim. Biophys. Acta* 1784(9):1146-1158.

7. Collman JP, *et al.* (1975) "Picket Fence Porphyrins." Synthetic Models for Oxygen Binding Hemoproteins. *J. Am. Chem.Soc.* 97(6):1427-1439.

8. Lecomte JTJ, Sukits SF, Bhattacharya S, & Falzone CJ (1999) Conformational properties of native sperm whale apomyoglobin in solution. *Protein Sci.* 8:1484-1491.

9. Feng Y & Sligar SG (1991) Effect of Heme Binding on the Structure and Stability of *Escherichia coli* Apocytochrome b_{562}. *Biochemistry* 30:10150-10155.

10. Dickerson RE, *et al.* (1971) Ferricytochrome c. *J. Biol. Chem.* 246(5):1511-1535.

11. Babul J & Stellwagen E (1972) Participation of the Protein Ligands in the Folding of Cytochrome c. *Biochemistry* 7:1195-1200.

12. Fisher WR, Taniuchi H, & Anfinsen CB (1973) On the Role of Heme in the Formation of the Structure of Cytochrome c. *J. Biol. Chem.* 248:3188-3195.

13. Ikai A, Fish WW, & Tanford C (1973) Kinetics of Unfolding and Refolding of Proteins II. Results for Cytochrome c. *J. Mol. Biol.* 73:165-184.

14. Kaminsky LS, Miller VJ, & Davison AJ (1973) Thermodynamic Studies of the Opening of the Heme Crevice of Ferricytochrome c. *Biochemistry* 12:2215-2221.

15. Tsong TY (1973) Detection of Three Kinetic Phases in the Thermal Unfolding of Ferricytochrome c. *Biochemistry* 12:2209-2214.

16. Stellwagen E & Babul J (1975) Stabilisation of the Globular Structure of Ferricytochrome c by Chloride in Acidic Solvents. *Biochemistry* 23:5135-5140.

17. Tsong TY (1975) An Acid Induced Conformational Transition of Denatured Cytochrome c in Urea and Guanidine Hydrochloride Solutions. *Biochemistry* 14:1542-1547.

18. Stellwagen E & Rysavy R (1972) The Conformation of Horse Heart Apocytochrome *c*. *J. Biol. Chem.* 247:8074-8077.

19. Bushnell GW, Louie GV, & Brayer GD (1990) High-resolution Three-dimensional Structure of Horse Heart Cytochrome c. *J. Mol. Biol.* 214:585-595.

20. Myer YP (1984) Ferricytochrome *c* and methionine 80-sulfur linkage. *J. Biol. Chem.* 259(10):6127-6133.

21. Broger C, Nałęcz MJ, & Azzi A (1980) Interaction of Cytochrome *c* with cytochrome bc_1 Complex of the Mitochondrial Respiratory Chain. *Biochim. Biophys. Acta* 592:519.

22. Graber EAE & Margoliash E (1990) Interaction of cytochrome *c* with cytochrome *c* oxidase: An understanding of the high- to low-affinity transition. *Biochim. Biophys. Acta* 1015:279-287.

23. Michel B & Bosshard HR (1984) Spectroscopic Analysis of the Interaction between Cytochrome *c* and Cytochrome *c* Oxidase. *J. Biol. Chem.* 259:10085-10091.

24. Smith HT, Ashmed AJ, & Millett F (1981) Electrostatic Interactionof Cytochrome *c* with Cytochrome c_1 and Cytochrome Oxidase. *J. Biol. Chem.* 256:4984-4990.

25. Taniguchi VT, Sailasuta-Scott N, Anson FC, & Gray HB (1980) Thermodynamics of Metalloprotein Electron-Transfer Reactions. *Pure Appl. Chem.* 52:2275-2281.

26. Santucci R, Reinhard H, & Brunori M (1988) Direct Electrochemistry of the Undecapeptide from Cytochrome *c* (Microperoxidase) at a Glassy Carbon Electrode. *J. Am. Chem. Soc.* 110:8537-8539.

27. Bixler J, Bakker G, & McLendon GL (1992) Electrochemical Probes of Potein Folding. *J. Am. Chem. Soc.* 114:6938-6939.

28. Latypov RF, Maki K, Cheng H, Luck SD, & Roder H (2008) Folding Mechanism of Reduced Cytochrome *c*: Equilibrium and Kinetic Properties in the Presence of Carbon Monoxide. *J. Mol. Biol.* 383:437-453.

29. Jones CM, *et al.* (1993) Fast events in protein folding initiated by nanosecond laser photolysis. *Proc. Natl. Acad. Sci. U.S.A.* 90:11860-11864.

30. Mines GA, Pascher T, Lee SC, Winkler JR, & Gray HB (1996) Cytochrome c folding triggered by electron transfer. *Chem. Biol.* 3:491-497.

31. Pascher T, Chesick JP, Winkler JR, & Gray HB (1996) Protein Folding Triggered by Electron Transfer. *Science* 271:1558-1560.

32. Churg AK & Warshel A (1986) Control of the Redox Potential of Cytochrome *c* and Microscopic Dielectric Effects in Proteins. *Biochem* 25:1675-1681.

33. Cohen DS & Pielak GJ (1995) Entropic Stabilization of Cytochrome *c* upon Reduction. *J. Am. Chem. Soc.* 117(6):1675-1677.

34. Dharmasiri K & Smith DL (1997) Regional Stability Changes in Oxidized and Reduced Cytochrome c Located by Hydrogen Exchange and Mass Spectrometry. *J. Am. Soc. Mass Spectrom.* 8:1039-1045.

35. Wand AJ, Roder H, & Englander SW (1986) Two-Dimension ^{1}H NMR studies of Cytochrome *c*: Hydrogen Exchange in the N-Terminal Helix. *Biochem* 25:1107-1114.

36. England JL, Pande VS, & Haran G (2008) Chemical Denaturants Inhibit the Onset of Dewetting. *J. Am. Chem. Soc.* 130:11854-11855.

37. Lim WK, Rosgen J, & Englander SW (2009) Urea, but not guanidinium, destabilizes proteins by forming hydrogen bonds to the peptide group. *Proc. Natl. Acad. Sci. U.S.A.* 106:2595-2600.

Chapter 4 – Conclusions

4 Conclusions and Future Work

The use of HDX-MS as a tool to study protein structure was demonstrated in this work. Both intact protein and spatially resolved analyses demonstrate the utility of this technique. Initial global studies can easily be conducted and if a difference is observed, one may proceed onto more localized analysis. In an experimental sense, global probing of the kinetics can cut down on unnecessary experiments. Furthermore, it allows the experimentalist to change experimental variables rather quickly, by using different solution conditions, ligands, or mutant variants. The application of this technique does come with a fair learning curve. Ensuring pH conditions remain the same, minimizing back-exchange, maintaining equilibrium during the exchange process, and analyzing peptic peptides are crucial to successful experiments. Ultimately though, at the root of any experiment, is a bottle of D2O and a way to measure the mass shift. It is this simplicity that makes this technique so powerful.

Chapter 2 highlighted the many reasons why HDX-MS is commonly used in research and in the pharmaceutical industry. The ability to monitor changes in protein structure and dynamics upon ligand binding is critical for drug design. Using Tε and Eε provided a system in which proteins from similar organisms with the same proposed binding site provided vastly different results upon exposure to a ligand. These results agreed well with the ligand affinity of the respective proteins using other analytical techniques and also revealed a previously unobserved dimeric form of Tε. Whether this form is physiologically relevant to the rest of the complex remains to be seen; however, future studies on the subunit especially in the presence of ATP must now take into account the possibility of protein dimerization. The analysis of a single subunit also begs the question whether the exchange kinetics observed would differ upon inclusion of the omitted complex.

The main objective of work in Chapter 3 was to determine the extent of structural change cytochrome c and its respective redox forms. In the presence of denaturant it was

possible to measure the steady increase in HDX coinciding with a progressive loss in stability. Though this structural change was observed, the small magnitude of the uptake made it difficult to push forward with spatially resolved data. Furthermore the internal structural fluctuations by re-oxidation of the Fe center made it difficult to predict the root cause of the exchange kinetics. Nonetheless this has laid the ground work in attempting to correlate exchange kinetics with that of kinetics arising from structural changes.

The size of the system which can be studied using HDX-MS is far greater than those presented in this work. It is the goal to expand HDX-MS by studying larger, more complex systems (1-3). The work done with ε can be extended by examining the εγ sub complex of F_1-ATPase, which has been reported to bind ATP (4). Therefore HDX-MS of εγ would determine the extent of the β-barrel protection observed upon dimerization versus in complex with the stator stalk. Building on this, the examination of the entire F_1-complex using HDX-MS would be truly remarkable; a task which would truly test both the experimentalist and the technique. The vast quantity of peptides as a result of peptic digestion alone is daunting, however the ability to piece together spatially resolved structural changes of what Paul Boyer adequately describes a "splendid" molecular machine would be indispensable (5). Intact protein work on F_OF_1-ATP synthase using high resolving mass spectrometers has recently been reported, including the ability to keep the complex from dissociating in the gas phase (6). It remains to be seen how the structure of these large complexes can be studied at amino acid resolution, although HDX-MS looks to be a promising candidate. The difficulty of studying F_1 under physiological conditions is due to the catalytic turnover of ATP, about $100s^{-1}$ (7). Therefore a regeneration system would have to be produced in order to study the complex. Possible ligand binding studies could include the use of adenosine 5'-γ-thiotriphosphate as an ATP analog (8). The thiol substitution on the γ-phosphate dramatically slows down the hydrolysis process. Building on the idea of examining F_1 it would be interesting to determine the structural changes of complexes from other organisms such as bovine or chloroplast F_1. This could assist in resolving the different regulatory mechanisms observed in each respective system.

From a well-studied protein in Cyt *c*, to the notion of examining the molecular machines of physiological systems, the future is bright for HDX-MS. It is the simplicity and versatility of this technique that makes it effective in examining the various systems discussed in the present writing. As the popularity and practice of HDX-MS grows, it will be intriguing to see its integration into other commonly used experimental procedures, or even more exciting, the creation of new analytical methods. Regardless of the system studied, there will always be one common factor; a simple bottle of heavy water.

4.1 References

1. Koshy SS, Eyles SJ, Weis RM, & Thompson LK (2013) Hydrogen Exchange Mass Spectrometry of Functional Membrane-Bound Chemotaxis Receptor Complexes. *Biochem* 52:8833-8842.

2. Mysling S, Betzer C, Jensen PH, & Jørgensen TJ (2013) Characterizing the Dynamics of α‑Synuclein Oligomers Using Hydrogen/Deuterium Exchange Monitored by Mass Spectrometry. *Biochem* 52(9097-9103).

3. Zhang H, Cui W, & Gross ML (2014) Mass spectrometry for the biopyhysical characterization of therapeutic monoclonal antibodies. *FEBS Lett.* 588:308-317.

4. Iizuka S, Kato S, Yoshida M, & Kato-Yamada Y (2006) γε sub-complex of thermophilic ATP synthase has the ability to bind ATP. *Biochem. Biophys. Res. Comm.* 349:1368-1371.

5. Boyer PD (1997) The ATP Synthase - A Splendid Molecular Machine. *Annu. Rev. Biochem.* 66:717-749.

6. Schmidt C, *et al.* (2013) Comparative cross-linking and mass spectrometry of an intact F-type ATPase suggest a role for phosphorylation. *Nat. Commun.* 4:1-11.

7. Etzold C, Deckers-Hebestreit G, & Altendorf K (1997) Turnover number of *Escherichia coli* F_0F_1 ATP synthase for ATP synthesis in membrane vesicles. *Eur. J. Biochem* 243:336-343.

8. Resetar AM & Chalovich JM (1995) Adenosine 5'-(γ-Thiotriphosphate): An ATP Analog That Should Be Used with Caution in Muscle Contraction Studies. *Biochem* 34:16039-16045.

Appendix 1 – Supporting Information

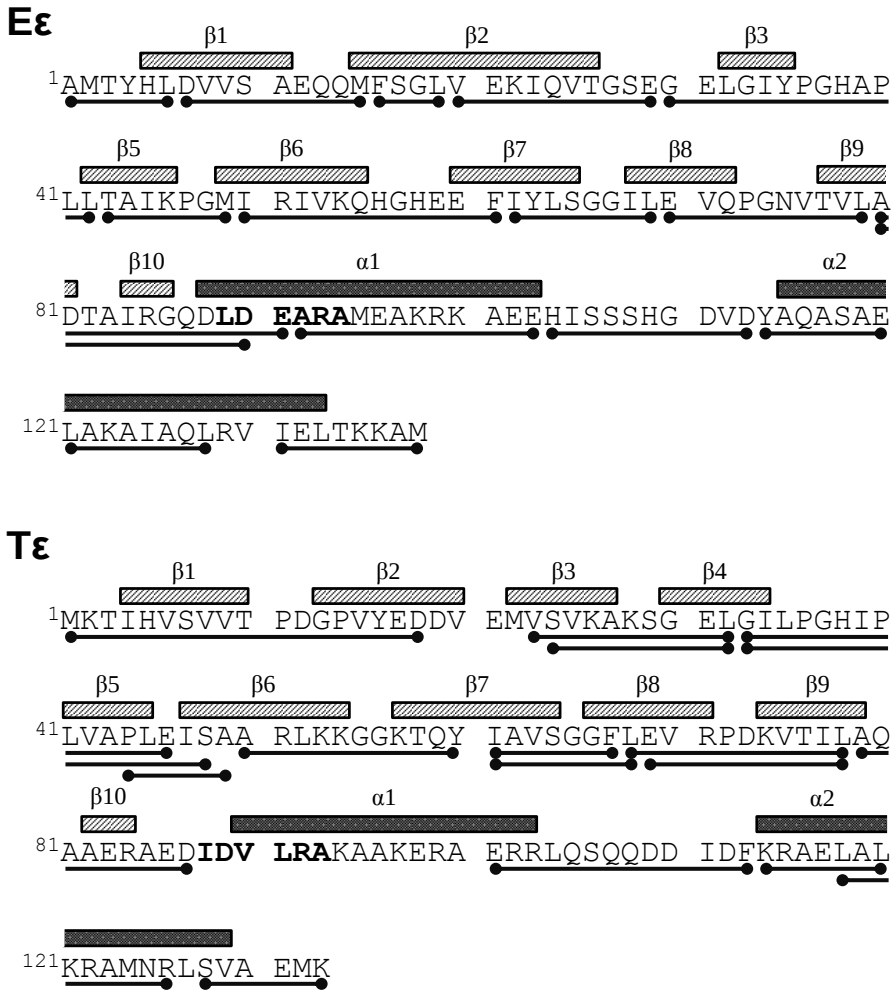

Figure S1. Sequence of Eε (top) (1) and Tε (bottom) (2). Secondary structure elements are indicated as boxes. The proposed I(L)DXXRA ATP binding motif (2) is highlighted in bold. Peptic peptides used for HDX are shown as solid lines below the sequence.

References

1. Uhlin U, Cox GB, & Guss JM (1997) Crystal structure of the ε subunit of the proton-translocating ATP synthase from *Escherichia coli*. *Structure* 5(9):1219-1230.

2. Yagi H, *et al.* (2007) Structures of the thermophilic F_1-ATPase ε subunit suggesting ATP-regulated arm motion of its C-terminal domain in F_1. *Proc. Natl. Acad. Sci. U.S.A.* 104:11233-11238.

Curriculum Vitae

Antony D. Rodriguez

Education

M.Sc. Physical/Analytical Chemistry
University of Western Ontario, London, ON — *2012-2014*

Thesis title: Protein Conformational Studies by Hydrogen/Deuterium Exchange Mass Spectrometry
Principle Investigator: Dr. Lars Konermann

B.Sc. Honors Spec. in Chemistry and Biochemistry
University of Western Ontario — *2008-2012*

Undergraduate Thesis: Exploring the Protein Electrospray Process by Electrostatic Modeling
Principle Investigator: Dr. Lars Konermann

Awards and Scholarships

Graduate Thesis Research Award – Departmental — *2013*

Support costs of research undertaken by graduate students that are directly related to the successful completed of their thesis requirements ($650)

Western Graduate Research Scholarship – Departmental — *2012-2013*

Support tuition costs of graduate students by their respective department ($3200 for two terms)

Dean's Honor List – Institutional — *2011-2012*

Achieved an 80% or above average throughout the academic year

Publications

1. **Rodriguez, A. D.**, Dunn, S. D., & Konermann, L. (2014). ATP-Induced Dimerization of the F_OF_1 ε Subunit from *Bacillus PS3*: A Hydrogen Exchange/Mass Spectrometry Study. (Submitted).

2. Konermann, L., Ahadi, E., **Rodriguez A. D.**, & Vahidi, S. (2013). Unraveling The Mechanism of Electrospray Ionization. *Anal. Chem.* **85**, 2-9.

3. Konermann, L., **Rodriguez A. D.**, & Liu, J. (2012) On the Formation of Highly Charged Gaseous Ions from Unfolded Proteins by Electrospray Ionization. *Anal. Chem.* **84**, 6798-6804.

Presentations

61nd ASMS Conference on Mass Spectrometry and Allied Topics *Jun 2013*

"ATP Binding to the ε Subunit of F_oF_1-ATP Synthase Monitored by HDX-MS" **Rodriguez, A. D.**, Dunn S. D., Konermann L.

25th Lake Louise Workshop on Tandem Mass Spectrometry *Nov 2012*

"Unraveling the mechanism of Electrospray Ionization" Konermann, L., Ahadi, E., **Rodriguez, A. D.**, Liu, J., Vahidi, S.

9th Annual Trent Conference on Mass Spectrometry *Aug 2012*

"On the formation of highly charged gaseous ions from unfolded proteins by electrospray ionization" **Rodriguez A. D.**, Liu, J., Konermann, L.

40th Southern Ontario Undergraduate Student Chemistry Conference *May 2012*

"Exploring the Protein Electrospray Process by Electrostatic Modeling" **Rodriguez, A. D.**, Liu, J., Konermann, L.